CORTEX 204 (2026) 336–356

Available online at www.sciencedirect.com

ScienceDirect

Journal homepage: www.elsevier.com/locate/cortex

Research Report

EEG signatures for tactile object individuation on a finger tip

Chunmiao Lou [a,1], Yang Lei [e,1], Uta Noppeney [f] and Lihan Chen [a,b,c,d,*]

[a] School of Psychological and Cognitive Sciences and Beijing Key Laboratory of Behavior and Mental Health, Peking University, Beijing, China
[b] Key Laboratory of Machine Perception (Ministry of Education), Peking University, Beijing, China
[c] National Engineering Laboratory for Big Data Analysis and Applications, Peking University, Beijing, China
[d] Beijing Key Laboratory of Brain-Computer Interface and Mental Health Modulation, China
[e] Mental Health Education Center, Zhengzhou University, Zhengzhou, Henan, China
[f] Donders Institute for Brain, Cognition and Behavior, Radboud University, Nijmegen, the Netherlands

ARTICLE INFO

Article history:
Received 10 February 2026
Revised 22 August 2026
Accepted 24 August 2026
Action editor Ryo Kitada
Published online 31 August 2026

Keywords:
Tactile enumeration
Object individuation
Neural decoding
N1000cc
tCDA

ABSTRACT

Object individuation (OI), i.e., segmenting sensory signals into individual objects based on spatial or temporal cues, has been studied predominantly in vision but remained largely unexplored in touch. Using EEG we studied the neural activity associated with OI in touch. In two experiments, participants (Experiment 1: n=28; Experiment 2: n=27) were presented with one to eight pins on their index fingertip. In Experiment 1, they enumerated the number of pins, a task relying on OI. In Experiment 2, they detected a brief temporal flicker in the tactile stimulus, a task that did not involve OI. Multivariate analyses showed that neural activity around 860 msec post-stimulus encoded the number of pins, but only during enumeration. Moreover, for Experiment 1, we observed that the amplitudes of two ERP indices, the late contralateral negativity (N1000cc) and the tactile contralateral delay activity (tCDA), increased with the number of enumerated items, peaking at three objects. Time-frequency analysis revealed greater oscillatory power in the alpha-band for small numerosities (1–3 items), corresponding to the range typically associated with tactile subitizing, relative to larger numerosities (4–6 items), suggesting an attentional control mechanism that aids in separating tactile objects from the background while reducing interference from irrelevant sensory information during capacity-limited OI processing. Importantly, these neural effects were not observed in Experiment 2. Collectively, our results provide evidence that tactile object individuation is capacity-limited and is associated with distinct N1000cc, tCDA, and alpha-band activity.

* *Corresponding author*. School of Psychological and Cognitive Sciences and Beijing Key Laboratory of Behavior and Mental Health, Peking University, Beijing, 100871, China.
E-mail address: CLH@pku.edu.cn (L. Chen).
[1] Co-first authors.

https://doi.org/10.1016/j.cortex.2026.08.014

Significance Statement

This study uncovers the neural correlates of object individuation (OI) in tactile enumeration, a domain where such mechanisms have remained largely uncharacterized. We identified two ERP markers—late contralateral negativity (N1000cc) and tactile contralateral delay activity (tCDA)—that track object quantity up to a capacity limit, providing direct evidence of limited-capacity processing in touch. Furthermore, we show that frontal-central alpha oscillations facilitate this process via attentional control. These findings suggest that tactile object individuation may rely on capacity-limited mechanisms that share important functional characteristics with those described in vision.

1. Introduction

In our everyday lives, we are frequently inundated with vast amounts of sensory signals, often surpassing our cognitive processing limits. To perceive specific objects effectively, it is essential to segregate task-relevant objects from background activity (Naughtin et al., 2017; Shea, 2020; Xu, 2009; Xu & Chun, 2009) – a process known as object individuation (OI) (Eger et al., 2009; Lou et al., 2022; Nieder et al., 2006; Nieder, 2025; Poncet & Chakravarthi, 2020; Pylyshyn, 1994; Shea, 2020). OI has been shown to develop at the very early stages during neurodevelopment (Ansari, 2008; Cicchini et al., 2016; Nieder, 2016). Individuals can typically segment approximately four objects. This capacity limitation in OI may explain cognitive processes such as subitizing (the rapid and accurate enumeration of four or fewer objects), multiple object tracking (MOT), and spatial working memory (Chesney & Haladjian, 2011; Drew, Horowitz, Wolfe, & Vogel, 2012; Drew & Vogel, 2008; Piazza et al., 2011; Xu, 2009) as uniformly limited to 4 objects.

Because information in the external environment is multisensory—such as pictures (visual), bird songs (auditory), and raised dots (tactile)—the OI process must be able to handle positional information from different modalities to meet the individual's needs for interacting with the external world. While vision is our primary sense for distance based parsing, tactile OI is essential for "proximal" interaction and manual dexterity. In everyday life, we frequently perform individuation without visual guidance—such as retrieving a specific coin from a pocket or manipulating fasteners on clothing—-where the brain must rapidly enumerate and distinguish contact points to plan motor output. Therefore, unlike early OI studies that mainly focused on the visual modality, in recent years an increasing number of researchers have started to investigate the OI process in the tactile modality (Cohen, Aisenberg, & Henik, 2018; Cohen, Arend, et al., 2018; Cohen & Henik, 2016; Gallace et al., 2006, 2008; Hochman et al., 2020; Lou et al., 2022;Tian & Chen, 2018). Furthermore, studying tactile OI allows us to determine whether the neural correlates of individuation (e.g., capacity limits and lateralized markers) are domain general across sensory systems or modality specific (Nieder, 2012).

Previous visual EEG research has associated two characteristic neural signatures with OI, the N2 posterior contralateral (N2pc) and the contralateral delay activity (CDA). Both N2pc and CDA have been linked with OI-related processes across a range of visual tasks, including subitizing (Pagano et al., 2014; Pagano & Mazza, 2012), visual working memory (Feldmann-Wüstefeld, 2021) and MOT task (Drew et al., 2012). During subitizing, the amplitudes of both N2pc and CDA increase with the number of individuated objects (1–4) (Mazza & Caramazza, 2011, 2015; Naughtin et al., 2016; Pagano et al., 2014). Similar load-dependent modulations have been shown in visual spatial working memory tasks (Feldmann-Wüstefeld, 2021; Göddertz et al., 2018; Li & Noguchi, 2022; Palva et al., 2011; Ward et al., 2021) and MOT tasks (Drew et al., 2012; Drew & Vogel, 2008), suggesting fundamental neural processes supporting capacity-limited object selection and maintenance that are shared across different visual OI contexts.

Subitizing has often been interpreted as a behavioral manifestation of OI. Rather than reflecting approximate estimation, successful enumeration within the subitizing range is thought to depend on the rapid segregation and parallel individuation of discrete objects (Mazza & Caramazza, 2015; Pylyshyn, 1994; Xu & Chun, 2009). This interpretation has been supported primarily in vision, where subitizing and OI share closely related behavioral capacity limits and neural signatures.

Whether similar individuation-related constraints operate in touch remains less clear. Prior tactile enumeration studies nevertheless suggest that tactile numerosity processing may also depend on object individuation-like mechanisms. The first evidence for tactile subitizing in passive touch using fingertip stimulation came from a study reporting high enumeration accuracy for set sizes of 1–3 simultaneously stimulated fingers, with markedly reduced performance for larger numerosities (Riggs et al., 2006). These findings were extended to active touch by a study showing that enumeration performance was substantially more efficient for up to three grasped objects than for larger sets, and that this advantage could not be explained solely by mass or volume cues (Plaisier et al., 2009). Subsequent studies further suggested that tactile numerosity processing is influenced by how tactile items are segmented and distributed across the hands and fingers (Plaisier et al., 2010; Plaisier & Smeets, 2011), consistent with the idea that tactile enumeration may be constrained by OI-related processes. However, not all studies have reported clear subitizing effects. For example, several studies using vibrotactile stimulation have reported little evidence for a robust tactile subitizing advantage, suggesting that tactile numerosity performance may depend strongly on stimulus characteristics and task demands (Gallace et al., 2006, 2008). Collectively, these findings suggest that tactile enumeration may involve capacity-limited individuation processes, although the underlying neural correlates remain largely unknown.

In addition to ERP components, alpha oscillations (8–12 Hz) also featured the OI-specific process. Within the OI range, alpha power has been shown to increase with the number of

enumerated objects in visual OI and working memory (Babu Henry Samuel et al., 2018; Hu et al., 2019; Jensen et al., 2002; Pavlov & Kotchoubey, 2022; Wianda & Ross, 2019; Wutz et al., 2020). This event-related synchronization (ERS) likely gates sensory input by inhibiting irrelevant visual information to protect/maintain memory representations from interference (Babu Henry Samuel et al., 2018; Hu et al., 2019). Load-dependent alpha modulation occurs during encoding (ERS peak increase) and retention (sustained ERS), primarily in right occipital and frontotemporal regions (Wianda & Ross, 2019). As memory load increases, alpha power rises during working memory delay periods over posterior cortical areas (Pan et al., 2018; Pavlov & Kotchoubey, 2022). Mechanistically, pulsatile alpha-band (~9–13 Hz) bursts in inferior parietal cortex, may signal rhythmic inhibitory control for object individuation within capacity limits (Jensen et al., 2002).

Despite this growing literature, the neural correlates of tactile OI remain comparatively underexplored. A theoretical link between OI and working memory follows naturally from how these two processes are thought to interact: once discrete objects have been segmented from the sensory input, their individuated representations must be briefly maintained while a response is prepared, and this maintenance stage is what the CDA and tactile contralateral delay activity (tCDA) are thought to index (Katus et al., 2015b; Vogel & Machizawa, 2004). Consistent with this account, CDA amplitude increases with the number of items held in working memory up to the individual's capacity limit, beyond which it plateaus because items exceeding that limit can no longer be individually maintained and are instead processed as an undifferentiated ensemble (Mazza & Caramazza, 2015; Vogel & Machizawa, 2004). Preliminary EEG evidence suggests that tCDA serves as a marker for tactile working memory, as its amplitude increases with memory load (Katus et al., 2015b). However, previous studies utilized limited load levels (1 *vs* 2 items), preventing a systematic assessment of whether tCDA reliably tracks tactile OI capacity. Beyond tCDA, tactile spatial attention is associated with the N2 central contralateral (N2cc, it is also referred to as N140 cc in some studies), a negative component reflecting attentional allocation and shifting between limbs or fingers (Forster et al., 2016; Gherri et al., 2021; Mena et al., 2020). Whether the N2cc also facilitates the OI process—particularly when stimuli are confined to a single fingertip—remains unknown.

The present study employs a single-fingertip stimulation paradigm to characterize the neural correlates of tactile OI. By contrasting conditions in which tactile object-based individuation was task-relevant versus task-irrelevant, we aim to distinguish neural activity associated with tactile individuation demands from activity related to shared low-level physical properties of the stimuli.

To this end, we investigated tactile OI mechanisms as indexed by contralateral ERP components and alpha-band oscillations. We conducted two EEG experiments. In Experiment 1, participants performed an OI-relevant, tactile enumeration task, specifically reporting the number of tactile pins presented simultaneously on their fingertip. For small numerosities, participants employed a subitizing strategy, which is based on OI processes. For large numerosities, in contrast, participants used an estimation strategy, which relies on the approximate number system (ANS) (Anobile et al., 2021;Burr et al., 2010; Dehaene & Changeux, 1993; Gallistel & Gelman, 1992). The ANS supports ensemble-level numerical representations. In Experiment 2, OI was rendered task-irrelevant to control for the influence of low-level physical attributes of tactile stimuli such as total area and perimeter across different OI conditions. Under this framework, we hypothesized that the amplitudes of late lateralized components reflecting the maintenance of individuated tactile representations would increase with the number of individuated pins within the tactile OI capacity range, and plateau or become variable once that range was exceeded, because items beyond the capacity limit can no longer be individually tracked and are instead processed via an approximate, ensemble-level strategy. This pattern was expected to emerge specifically when OI was task-relevant, that is, in the enumeration task but not in the control discrimination task. Furthermore, we predicted stronger (parietal) alpha power within the subitizing range (i.e., within the OI range, 1–3) compared to outside the subitizing range (i.e., outside the OI range, 4 and above), reflecting enhanced inhibitory demands. Specifically, during the OI process, the alpha oscillation suppresses interfering stimuli and directs attention to the positions that require prioritized selection and processing, thereby achieving a better separation of the target objects from the background.

2. Materials and methods

2.1. Participants

We performed a priori sample size estimation using G*Power 3.1 (Faul et al., 2007) based on the medium effect size ($f = .25$) of the effect of numerosity, with a significance level of $\alpha = .05$ and a power of .8. With a within-subject design comprising three levels (numbers 1–3 and numbers 4–6), a total of 28 participants was required. Accordingly, we recruited 30 participants for Experiment 1 (15 males; mean age = 21.6 ± .63 years), and obtained 28 valid datasets. Two participants were excluded because their response rates exceeded three standard deviations from the group mean. In Experiment 2, we recruited 28 participants (16 males; mean age = 21.5 ± .33 years), and collected 27 valid datasets. All participants had normal or corrected-to-normal vision and reported no known neurological disorders. The experiments were conducted in accordance with the institutional guidelines approved by the Academic Affairs Committee of the School of Psychological and Cognitive Sciences at Peking University, China. All participants provided written informed consent prior to the experiment and received reimbursement for their participation.

2.2. Stimuli and apparatus

We used a Piezo stimulator (QuaeroSys, Germany) equipped with 20 tactile pins with a maximal refresh rate of 1 kHz, to deliver tactile stimulation. The tactile pins were arranged with a minimum inter-distance of 2.5 mm. Their intensities and durations could be individually controlled with MATLAB

(MathWorks Inc.) and Psychophysics Toolbox (Brainard, 1997; Kleiner et al., 2007; Pelli, 1997). For both experiments, we set the intensity to the maximum level for all tactile pins. A 15-inch Dell LCD monitor (1336 × 768 pixels, 60 Hz frame rate) was used to display fixation points and instructions.

2.3. Experiment 1: behavioral task of tactile enumeration with OI

Experiment 1 consisted of two blocks. Across the two blocks, the left and right hands served as the target hand once each, with block order counterbalanced across participants. Before starting each block, participants were informed which hand was the target hand. Each trial started with a fixation point displayed at the center of the screen for a duration of 500–1000 msec (the timing was randomly jittered, with a mean of 750 msec), followed by a blank screen lasting 500 msec. Subsequently, tactile pins (varying in number from 1 to 8) were simultaneously presented on both forefingers for 1500 msec. Following the disappearance of the stimuli, a question appeared on the screen after a 2-s delay. Participants reported the number of tactile pins by pressing the corresponding key (1–8) on a numeric keypad positioned centrally between the two hands. Following the question, participants entered their response and then returned both hands to the tactile stimulators before the next trial. For each participant, responses were always made either with the hand ipsilateral to the target hand or with the hand contralateral to the target hand, and this assignment was counterbalanced across participants. Because the target hand was counterbalanced across blocks, all participants used both hands equally often across the experiment.

To ensure that participants followed the instructions and focused on the tactile stimuli on the target side for accurate reporting, rather than randomly selecting a side, we designed the trials as follows: In half of the trials, the non-target tactile stimuli exactly matched those on the target side in both quantity and position. In the remaining half, the non-target tactile stimuli were presented randomly and did not match the target side.

Each block consisted of 336 trials, comprising a 2 (Congruency: congruent *vs* incongruent) × 8 (Number of tactile pins: 1–8) factorial design, with 21 repetitions per condition. This resulted in a total of 672 trials for the entire experiment. Prior to the formal test, participants completed 20 practice trials to familiarize themselves with the procedure (Fig. 1).

2.4. Experiment 2: behavioral task of target discrimination without OI

In Experiment 2, participants were presented with the same stimuli in a target detection task that did not involve OI, except that some trials included a flicker in the stimuli. Participants decided whether the tactile pins on the target side were 'flickering', i.e., briefly interrupted. In the flickering condition, the tactile stimuli were presented for 500–800 msec, stopped for 100 msec, and then reappeared for 600–900 msec. In the non-flickering condition, the stimuli were presented throughout the 1500 msec duration, as in Experiment 1. The trial arrangement for the right hand as the target side is detailed in Table 1. The remaining design and procedure of Experiment 2 were aligned with those of Experiment 1. Participants responded using a two-button response device positioned centrally between the two hands. One button indicated "flicker present" and the other indicated "flicker absent". Response-hand assignment (ipsilateral versus contralateral relative to the target hand) and button-response mapping were counterbalanced across participants. For subsequent data analysis, we exclusively used data from trials where neither the target side nor the opposite side exhibited flickering conditions, as these conditions matched those of Experiment 1.

2.5. EEG data acquisition and preprocessing

Continuous electroencephalogram (EEG) data were recorded using a 64-electrode actiCAP from Brain Products (Munich, Germany) at a sampling rate of 1000 Hz. The reference electrode was positioned at FCz, and the ground electrode was at AFz. Electrode impedances were kept below 10 KΩ. Participants were seated in a comfortable chair within a quiet, temperature-controlled room and were instructed to attend to the stimuli while keeping their muscles relaxed. A vertical electrooculogram (EOG) was additionally recorded using an electrode placed below the participant's right eye. Offline EEG analysis was performed using the EEGLAB Toolbox for MATLAB (Delorme & Makeig, 2004) and custom-written MATLAB functions. The signals were first re-referenced to the average of the left and right mastoids, and a band-pass filter was applied with a frequency range of .1–40 Hz. EEG epochs were extracted using a 3000-msec window, spanning 500 msec before and 2500 msec after stimulus onset. The average signals were normalized to a baseline corresponding to the average amplitude from −500 to 0 msec. Data with major muscle noise or voltage issues were visually inspected and removed. Furthermore, independent component analysis (ICA) was employed to manually eliminate prominent artifacts such as blinks, saccades, cardiovascular-related signals, and persistent muscle noise.

2.6. Overview of behavioral and EEG analysis

Before describing the analysis approach, it is necessary to specify the numerosity conditions included in each analysis. Behavioral analyses were conducted across all eight numerosity levels (1–8). EEG analyses, however, were restricted to conditions 1–6 for the following reasons. Conditions 7 and 8 were excluded from EEG analyses due to complementary methodological and interpretational considerations. For condition 7, mean error rates exceeded 75% in a substantial proportion of participants (M = 76.7%, SE = 2%), resulting in a limited number of correct trials after preprocessing and artifact rejection, which reduced the reliability of ERP and multivariate pattern analysis (MVPA) estimates. For condition 8, performance is influenced by range-end effects commonly observed in enumeration tasks, whereby awareness of the stimulus range can attenuate errors at extreme numerosities (Burr et al., 2010; Piazza et al., 2011), making this condition less interpretable as a measure of genuine numerosity processing.

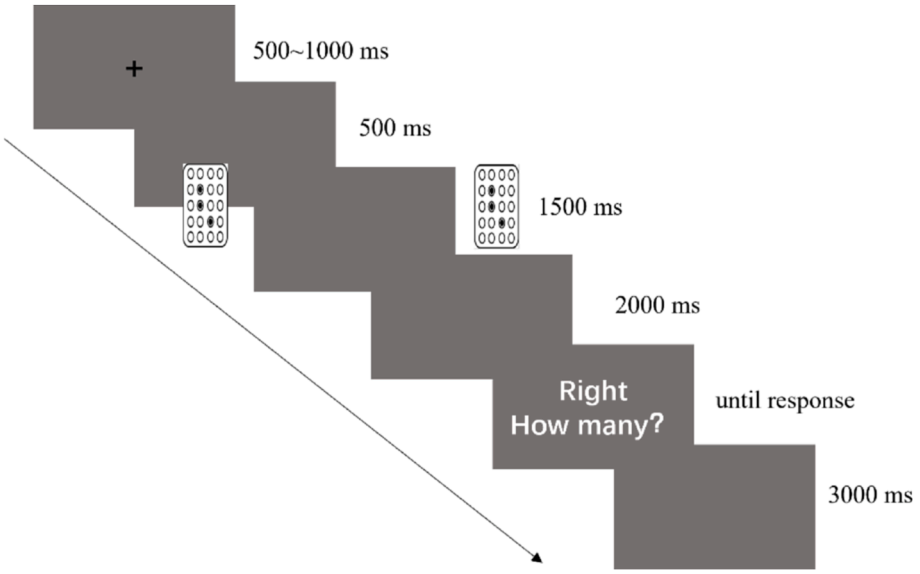

Fig. 1 – Tactile enumeration paradigm in Experiment 1. In this example trial, participants received congruent tactile stimulation to both hands and reported the perceived number of tactile pins on the target hand (i.e., right hand). Here for illustration purposes, the numerosity level was 3, the actual range varied from 1 to 8.

Table 1 – Arrangement of trials in experiment 2 when the right hand is the target.

	Target side flickering	Target side non-flickering
Non-target side flickering	16 ($2^{a} \times 8^{b}$)	16
Non-target side non-flickering	16	288 ($2 \times 8 \times 18^{c}$)

[a] Target hand: right hand or left hand.
[b] The number of tactile pins:1–8.
[c] Repetition times.

All subsequent EEG analyses therefore refer to conditions 1–6 only.

Studies using enumeration tasks to investigate visual OI have suggested logistic function fitting as an efficient way to determine the OI range (Anobile et al., 2019; Piazza et al., 2011). Following these previous studies, we also fitted a logistic function to each participant's error rates in the enumeration task, and the inflection point of the fitted function was taken as the OI capacity. The inflection point was defined as the point at which the second derivative of the logistic function equaled zero. The fitting results indicated an OI capacity of 2.99 in our experiment (SE(capacity) = .10; average R^2 = .98, $SE(R^2)$ = .02). Therefore, in our analysis, the OI range was classified as 1–3 and the range outside OI, we used conditions 4–6 to serve as a comparison. The boundary between within-OI and outside-OI ranges was defined at 3 items, consistent with the previous tactile enumeration literature (Plaisier et al., 2009; Plaisier & Smeets, 2011; Riggs et al., 2006), which consistently reports a reduced capacity-limited individuation range in touch relative to vision.

Drawing on the ERP decoding results from Experiments 1 and 2, we first identified candidate temporal intervals associated with tactile OI by examining time periods in which decoding accuracy in Experiment 1 significantly exceeded chance level (cluster-based permutation test, $p < .05$), while no corresponding significant clusters were observed in Experiment 2 under the same statistical threshold. This cross-experiment dissociation was used as a functional constraint to separate stimulus-driven processing (shared across tasks) from task-dependent OI-related processing. To further ensure consistency with prior literature, the resulting candidate intervals were evaluated against previously reported temporal ranges of late contralateral components in tactile working memory, including the tCDA (Katus & Eimer, 2015a; Katus et al., 2015b). Constrained by the convergence of cross-experiment decoding dissociation and prior empirical findings, we selected two a priori-defined analysis windows: 900–1200 msec, corresponding to a late contralateral negative component (N1000cc), and 1500–1800 msec, corresponding to the tCDA.

Within these windows, contralateral-minus-ipsilateral difference waves were computed following established procedures used in tactile lateralized ERP studies (Forster et al., 2016; Gherri et al., 2021; Mena et al., 2020). The resulting difference waves were used to quantify the N1000cc and tCDA components. Peak latencies and amplitudes were measured from a lateral centroparietal electrode cluster (FC3/4, FC5/6, C3/4, C5/6, CP3/4, and CP5/6), consistent with previous studies of tactile CDA (Katus & Eimer, 2015a; Katus et al., 2015b). A one-way repeated-measures ANOVA was conducted to compare the amplitudes across different numerosity levels within (1–3) and outside (4–6) the OI range, followed by post-hoc Tukey's pairwise comparisons if a significant main effect was observed.

For time-frequency analysis, time-frequency distributions of EEG trials were obtained using a short-time Fourier transform (STFT) with a fixed 250 msec Hanning window (Hu et al., 2014; Tu et al., 2016). The time domain extended from −500 to 2500 msec in 1 msec steps, while the frequency domain spanned from 1 to 30 Hz in 1 Hz steps.

Spectrograms were corrected by subtracting the average power within the pre-stimulus reference interval (−400 to −100 msec) for each frequency. Based on previous findings (Esmaeili & Diamond, 2019; Gui et al., 2017; Su et al., 2020) and topographic maps, three regions of interest (ROIs) were identified for analyzing alpha power: the frontal (F cluster: F1, F2, Fz, AF3, AF4), central (C cluster: FC1, FC2, C1, Cz, C2), and parieto-occipital (P cluster: POz, PO3, PO4, P1, P2) regions.

2.7. EEG multivariate pattern analysis (decoding analysis)

To examine whether tactile OI load could be decoded from neural population activity, we performed MVPA on EEG data. The decoding target was the numerosity of tactile pins, and decoding was performed separately at each time point based on the spatial distribution of signals across the scalp. Two signal types were analyzed independently: the phase-locked ERP voltage and the phase-independent alpha-band (8–12 Hz) EEG power. Only correct trials were included in the analyses. In Experiments 1 and 2 we employed the same decoding approach.

Decoding analyses were conducted separately for numerosities within the OI capacity range (numerosities 1, 2, and 3) and outside the OI capacity range (numerosities 4, 5, and 6). Consequently, each decoding analysis constituted a three-class classification problem (i.e., distinguishing between 1, 2, and 3; or between 4, 5, and 6). We performed four such decoding analyses in total: decoding within the OI range using ERP signals, decoding within the OI range using alpha band signals, and decoding outside the OI range using both ERP and alpha band signals.

EEG data were resampled at 100 Hz to enhance computational efficiency, resulting in a temporal resolution of 10 msec per time point. Decoding was performed independently at each of the 249 time points ranging from −500 msec to 1980 msec relative to the onset of target stimulation. Prior to each analysis, a 4-dimensional data matrix (dimensions: time, number of tactile pins, correct trials, and electrode site) was generated for each participant.

The decoding procedure followed a similar approach to Bae and Luck (2018, 2019). A combination of a Support Vector Machine (SVM) and Error-Correcting Output Codes (ECOC) (Dietterich & Bakiri, 1994), a standard multiclass classification framework that decomposes a multiclass problem into multiple binary classifiers, was utilized to classify the numerosity of tactile pins based on the spatial distribution of signals across 61 scalp electrodes. Specifically, for each three-class numerosity problem, the ECOC framework decomposed the task into three binary one-versus-all classifiers (e.g., 1 *vs* [2, 3]; 2 *vs* [1, 3]; 3 *vs* [1, 2]).

Decoding was performed using threefold cross-validation at each time point. Trials were randomly divided into three subsets, with two subsets used for training and the remaining subset used for testing. To train an unbiased SVM, we balanced the number of trials across the training and testing subsets via resampling. Specifically, we randomly selected trials from the condition with more trials to match the trial count of the condition with fewer trials. This procedure was repeated 10 times, and the average decoding accuracy was calculated for each time point. For each cross-validation fold, the trained SVM-ECOC model predicted the numerosity of the held-out averaged patterns. Final class labels were assigned by choosing the class that minimizes the average binary loss across the three SVMs. A prediction was considered correct only if it exactly matched the true number.

This decoding procedure was repeated 10 times with different random trial assignments, resulting in 90 decoding iterations at each time point (3 numerosities × 3 cross-validations folds × 10 repetitions). Decoding accuracy was averaged across iterations for each participant and time point. Chance level accuracy was .333 given three equiprobable numbers.

2.8. Statistical analysis of decoding accuracy

Statistical inference on decoding accuracy followed a cluster-based permutation approach (Groppe et al., 2011). At each of the 249 time points, a one-sample one-tailed *t*-test assessed whether group-level decoding accuracy exceeded chance (1/3). Contiguous time points with $p < .05$ (uncorrected) were identified and grouped into clusters; the cluster-level statistic was defined as the sum of t-values across all member time points. To construct a null distribution, condition labels were randomly permuted 10,000 times; for each permutation, the same clustering procedure was applied and the maximum cluster mass was recorded. A cluster was considered significant if its observed mass exceeded the 95th percentile of this null distribution ($\alpha = .05$, family-wise error rate controlled across the full time dimension). Classification was performed on the raw 61-channel EEG voltage (ERP decoding) or alpha-band power values (time-frequency decoding) at each time point without prior dimensionality reduction; the 61 electrode values at each time point constituted the feature vector.

2.9. Time generalization

To assess the temporal consistency of the decoding signal, a temporal generalization matrix was utilized, following King and Dehaene (2014). A classifier trained at one time point was tested across all 249 time points, yielding a 249 × 249 decoding accuracy matrix. Statistical significance in the 2D matrices was assessed using a two-tailed *t*-test against chance classification for each time point, with False Discovery Rate (FDR) correction applied for multiple comparisons. To prevent underestimating the mean generalization time, only the time window in which the diagonal classifiers performed above the chance level was included in the analysis. This analysis

determines whether the neural code is stable or dynamically evolving. Based on this rationale, if a stable neural coding pattern exists, the generalization results would reveal a significant square-shaped region, with the side length of the square reflecting the duration of that stable neural pattern.

3. Results

3.1. Behavioral results

In previous studies (Anobile et al., 2012; Burr et al., 2010), error rate and Weber fraction have been widely used as dependent measures to assess enumeration performance and to differentiate between subitizing and estimation. Relative to estimation, subitizing is generally associated with lower error rates and greater precision. Accordingly, in the behavioral analysis of Experiment 1, we employed both of these dependent variables. The rationale for using the Weber fraction rests on a simple distinction: ANS-based estimation follows scalar variability, so the Weber fraction stays roughly constant across set sizes, whereas object individuation yields near-exact representations that depart from this pattern. A low, non-constant Weber fraction was therefore taken as evidence of individuation-based processing, and a stable, Weber-law-consistent fraction as evidence of estimation-based processing (Burr et al., 2010).

We performed a 2 (target hand: left, right) × 2 (congruency: congruent *vs* incongruent) × 8 (numerosity: 1–8) repeated-measures ANOVA[2] test on the error rate (ERR) of Experiment 1. There was a significant main effect of numerosity ($F_{(3.315,\ 89.509)} = 208.519$, $p < .001$, $\eta^2_p = .885$), indicating that ERR gradually increased with the increase of the target number (Fig. 2). Post-hoc tests revealed significant differences between all numbers except for 4 and 8, 5 and 8, and 6 and 8 ($ps < .05$). The main effect of the target hand was not significant, indicating no significant difference in enumeration performance between the left and right hands. More importantly, there was no significant difference in error rate between congruent and incongruent conditions, suggesting that participants selectively attended to the target hand as instructed.

To further examine the precision of tactile numerosity judgments, Weber fractions were calculated for each numerosity by dividing the standard deviation of participants' responses by the perceived numerosity. A repeated-measures ANOVA revealed a significant main effect of numerosity on Weber fraction ($F_{(2.11,\ 57.03)} = 12.76$, $p < .001$, $\eta^2_p = .321$). Bonferroni-corrected pairwise comparisons showed that Weber fractions for one and two items were significantly lower than those for three and four items (all $ps < .003$). In contrast, Weber fractions did not differ significantly among numerosities three through seven in most comparisons, indicating a relatively stable level of variability across larger numerosities. As shown in Fig. 2, Weber fractions increased from one to approximately three items and then remained relatively constant across higher numerosities. This pattern is consistent with a transition from a high-precision small-number regime to a larger-number regime characterized by approximately constant Weber fractions.

In Experiment 2, we used error rate as the dependent variable. Given the simplicity of the experimental task, participants' error rates showed a floor effect ($M = .0489$, $SE = .00105$). This restricted range of variability violated the assumption of homogeneity of variance and provided insufficient sensitivity to detect differences across numerosity conditions. Consequently, no statistical analyses were performed on the error rate data.

3.2. ERP decoding

In Experiments 1 and 2, multivariate decoding analyses were conducted on ERP activities to classify different target numerosities, separately within the OI range (1–3) and outside the OI range (4–6). The results indicated that decoding accuracy significantly exceeded the chance level beginning at 320 msec after the target was presented (cluster $p < 10^{-4}$), within the OI range of Experiment 1, indicating that different numerosity levels could be distinguished according to participants' ERP signals starting from 320 msec (see Fig. 3A).

However, the successful classification of different numerosity levels at early latencies does not necessarily imply engagement of OI-specific processes. Instead, early decoding may reflect stimulus-driven neural encoding that is sensitive to non-numerical physical properties of the tactile stimuli, such as differences in total stimulated area or spatial configuration, which covary with numerosity. To disentangle stimulus-driven encoding from task-dependent OI-related processes, we directly compare the decoding results between Experiment 1 and 2. In Experiment 2, participants performed a target discrimination task that did not require explicit individuation of multiple tactile items. As shown in Fig. 3C, within the OI range of Experiment 2, decoding accuracy was significantly higher than chance level from 320 msec to 860 msec (cluster $p < 10^{-4}$), closely overlapping with the early decoding interval observed in Experiment 1. This convergence suggests that decoding during this early time window reflects stimulus-driven encoding of non-numerical physical stimulus features that is expressed irrespective of task demands.

Critically, beyond 860 msec, decoding accuracy remained significantly above chance only in Experiment 1, but not in Experiment 2. This dissociation indicates a transition from stimulus-driven encoding to task-dependent neural processes specifically associated with tactile OI. Accordingly, the high decoding accuracy observed beyond 860 msec in Experiment 1 can be largely ascribed to OI processing rather than to non-numerical physical stimulus properties. Hence, the temporal window for ERP components associated with tactile OI processes should be considered to commence after 860 msec following the presentation of tactile stimuli. This timing allows for the minimization of the influence of non-numerical physical stimuli processing on ERP component amplitudes.

[2] In each ANOVA of each experiment, the Bonferroni correction for multiple comparisons was used in post-hoc tests. Whenever the Sphericity assumption was violated, we applied the Greenhouse-Geisser correction in each ANOVA.

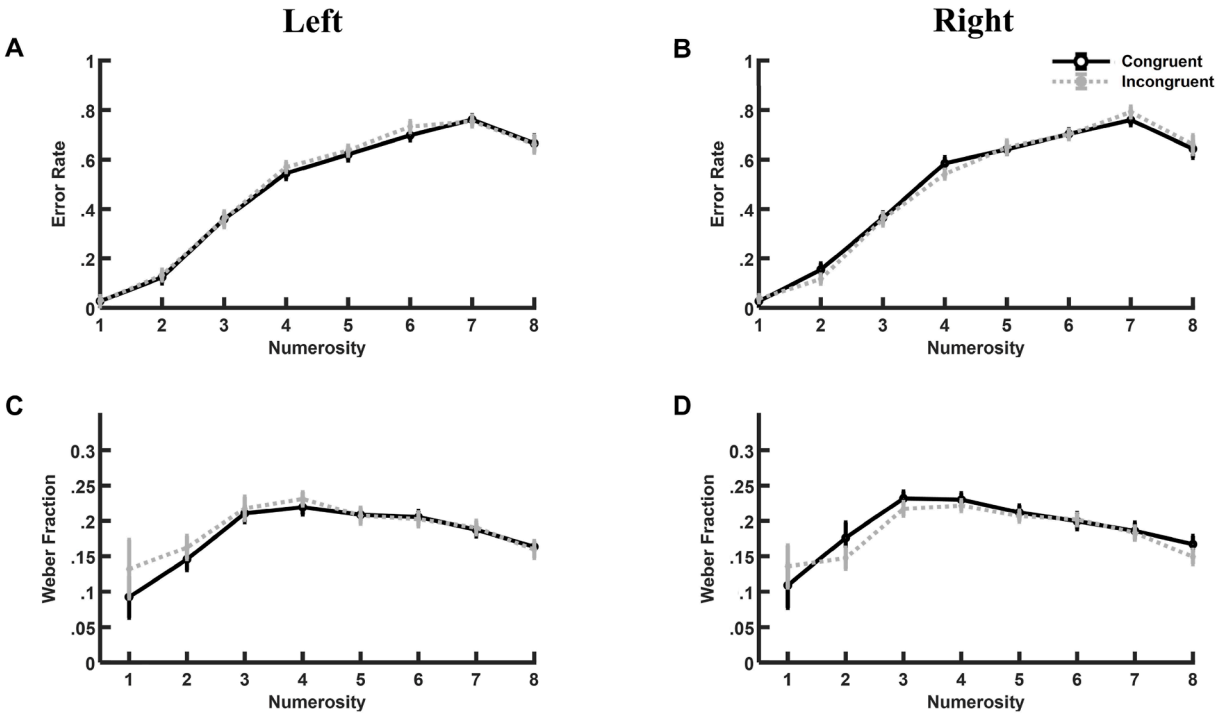

Fig. 2 – Behavioral results of Experiment 1. (A) Enumeration error rates for Experiment 1 when the target hand was left. (B) Enumeration error rates for Experiment 1 when the target hand was right. (C) Weber fractions when the target hand was the left hand. (D) Weber fractions when the target hand was the right hand. Weber fractions were calculated as the standard deviation of participants' responses divided by the perceived numerosity. Black curves represented the conditions whose non-target tactile stimuli were congruent with those on the target side. Gray curves represented incongruent conditions. Error bars denoted the standard errors of the mean.

Consistent with this interpretation, the decoding accuracy outside the OI range in both Experiments 1 and 2 did not significantly exceed chance level. This finding reinforces the conclusion that the high decoding accuracy observed within the OI range (after 860 msec in Experiment 1) is primarily attributable to OI processing rather than the impact of non-numerical physical stimulus factors.

3.3. *ERP time generalization*

Based on the decoding outcomes from Experiments 1 and 2, the time window of 320–2000 msec within the OI range of Experiment 1 can be segmented into two distinct phases. The initial phase, spanning from 320 msec to 860 msec, is characterized by successful classification of different numerosity levels, which may be partially attributed to variations in non-numerical physical stimuli across these levels. The subsequent phase, from 860 msec to 2000 msec post-stimulus presentation, is marked by high decoding accuracy predominantly resulting from OI processing (Katus et al., 2015b).

To substantiate our interpretation, we constructed a temporal generalization matrix for each decoding instance (Fig. 4). Our expectation was to identify two relatively stable neural code patterns corresponding to the aforementioned phases. Specifically, we anticipated observing two significant square-like regions in the generalization results of Experiment 1. It should be noted that the 320–860 msec window reflected a combined influence of non-numerical physical stimulus processing and OI processes, whereas the 860–2000 msec window was predominantly driven by OI processes. OI processes were present throughout the entire 320–2000 msec period. Because OI processes existed in both phases, additional significant generalization regions appeared at the junction between the two square clusters in our time-generalization results, as indicated by the areas outside the green box in Fig. 4. In Experiment 2, we expected to find one stable pattern, represented by a significant square-like region (see the green squares in Fig. 4). The results largely aligned with our expectations, and the boundaries of the two square regions in the generalization results of Experiment 1 indeed occurred around 860 msec, as hypothesized.

3.4. *N1000cc and tCDA*

In Experiment 1, we employed bilateral central area electrodes, specifically FC3/4, FC5/6, C3/4, C5/6, CP3/4, and CP5/6, to compute the ERP amplitudes on both the ipsilateral and contralateral sides relative to the target. To mitigate the impact of early stimulus-driven sensory encoding related to non-numerical physical stimulus attributes, we deliberately

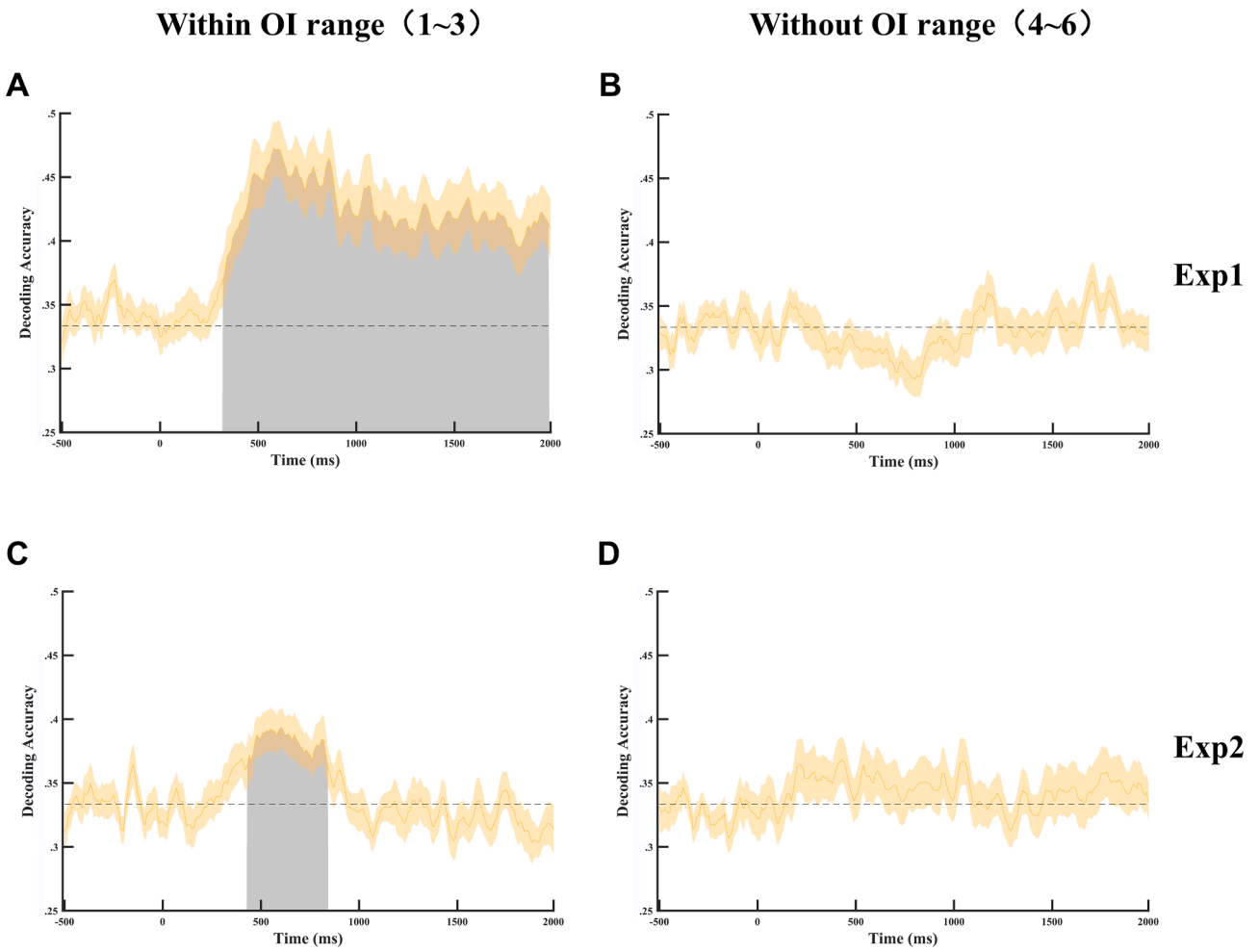

Fig. 3 – Decoding accuracies based on ERP signals for Experiment 1 and Experiment 2. Left panels showed the decoding accuracy within the OI range using ERP amplitude under 1–3 conditions from Experiment 1 (A) and Experiment 2 (C). Right panels showed decoding accuracy outside the OI range using ERP amplitude under 4–6 conditions from Experiment 1 (B) and Experiment 2 (D). The black dashed line represented the chance level of 1/3. Shaded regions around decoding accuracy curves represent 95% confidence intervals across participants. Gray shading indicated time points with significant cluster permutation results.

excluded the early component N2cc, which peaks around 100–300 msec, from further analysis.

Nonetheless, we conducted additional analyses on the N2cc to examine whether an early lateralized negativity analogous to the N2cc (Katus et al., 2015b) was detectable in the present data. Given the sustained 1500 msec stimulus duration used here, which differs substantially from the brief stimuli in the original N2cc paradigm, we defined an analysis window of 250–550 msec post-stimulus onset as the most analogous time range (see Supplementary Fig. S1). A one-sample *t*-test against zero confirmed a significant contralateral-minus-ipsilateral negativity ($t(27) = -6.756$, $p < .001$, Cohen's $d = 1.278$). We conducted two separate one-way repeated measures ANOVAs for the OI range (1–3) and outside the OI range (4–6). A significant main effect of numerosity was observed within the OI range ($F_{(2, 54)} = 6.122$, $p = .004$, $\eta^2_p = .185$). In contrast, no significant effect was found outside the OI range ($F_{(2, 54)} = .076$, $p = .927$) (post-hoc comparisons see Supplementary Fig. S2).

Leveraging the ERP decoding results and the peak distribution among participants, we identified two pertinent time windows: 900–1200 msec and 1500–1800 msec. We then calculated the difference in average amplitude between electrodes on the contralateral side and those on the ipsilateral side of the target. A one-sample *t*-test against zero revealed significant negative components within both time windows (900–1200 msec: $t(27) = -6.219$, $p < .001$, Cohen's $d = 1.175$; 1500–1800 msec: $t(27) = -5.867$, $p < .001$, Cohen's $d = 1.109$). We designated these two lateralized negative components as N1000cc and tCDA, respectively (see Fig. 5).

We compared the N1000cc's amplitudes of conditions 1 to 6 with a repeated-measures ANOVA and found a significant main effect of numerosity($F_{(2.774, 74.899)} = 5.559$, $p < .001$, $\eta^2_p = .171$). Post-hoc analysis showed significant differences between 1 and other number levels (*p*s < .05). We observed a positive correlation between numerosity and the amplitude

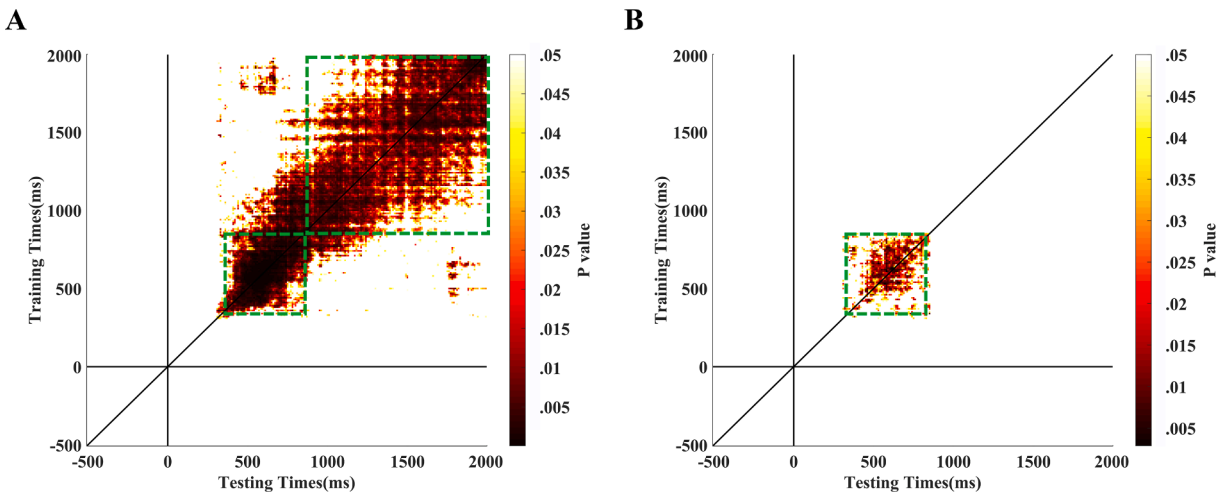

Fig. 4 – Time generalization results of ERP signals for Experiment 1 (A) and Experiment 2 (B). Highlighted time points represented clusters that were significant after FDR correction. The significant square-shaped regions indicated a stable neural coding pattern, with the side length of the square representing the duration of that pattern. Green squares are only shown for illustration.

of N1000cc within the OI range of 1–3. As the numerosity increased, the amplitude of N1000cc correspondingly increased, reaching its peak around a numerosity of 3. However, starting from a numerosity of 4, the amplitude of N1000cc began to exhibit fluctuations around this peak value. To visually illustrate the difference in N1000cc amplitude changes within and outside the OI range, we divided numerosity levels into two ranges: 1–3 and 4–6. Further analysis within the OI range (1–3) showed a significant main effect of numerosity ($F_{(1.319,\ 35.609)} = 14.260$, $p < .001$, $\eta^2_p = .346$). Post-hoc analysis indicated significant differences between 1 ($M = -2.006$, $SE = .433$) and 2 ($M = -3.365$, $SE = .572$) (t (27) = 3.479, $p = .005$, Cohen's $d = .657$), 2 and 3 ($M = -4.014$, $SE = .655$) (t (27) = 2.818, $p = .027$, Cohen's $d = .532$), and 1 and 3 (t (27) = 4.132, $p = .001$, Cohen's $d = .781$). As the numerosity increased, the amplitude of N1000cc gradually increased. However, when analyzing data outside the OI range, we observed no significant main effect of numerosity (p .05). This finding suggests that there is no positive correlation between the

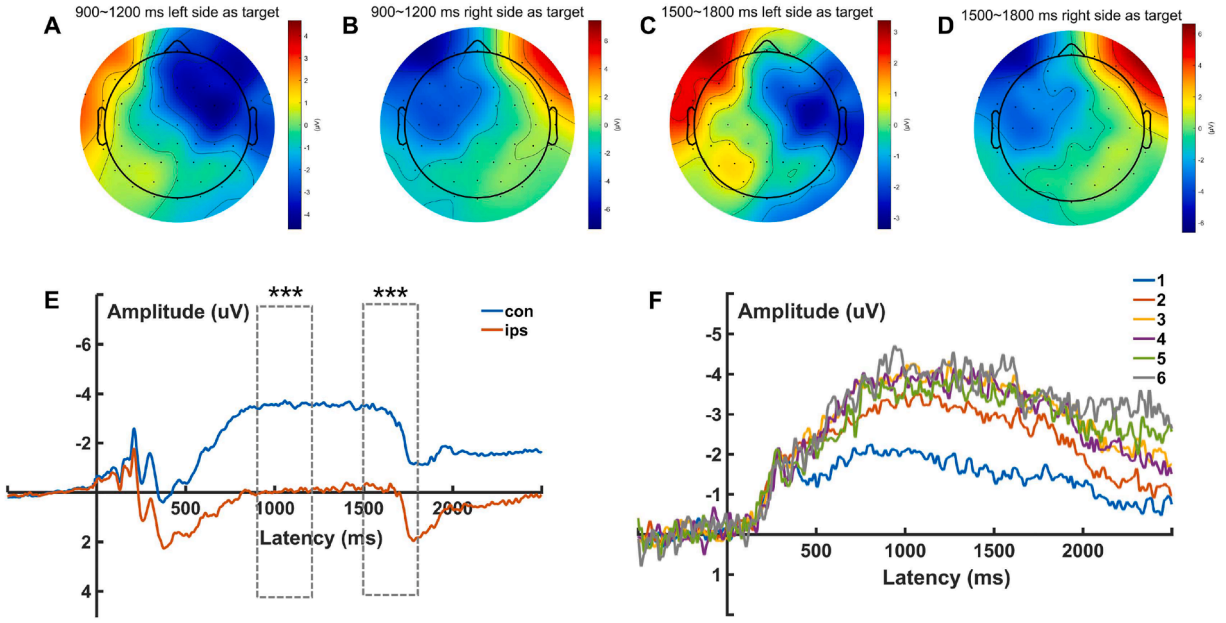

Fig. 5 – ERP results for Experiment 1. (A–D) Scalp distributions of ERP amplitude for different time windows and target conditions. (E) Differences in ERP amplitudes between contralateral and ipsilateral target sides at the central electrodes. The blue and red curves represented the average amplitudes of 1~6 for contralateral and ipsilateral target sides. (F) Difference wave amplitudes for the 1–6 levels at the central electrodes. Difference wave was defined as the amplitude difference between contralateral and ipsilateral target sides. *$p < .05$, **$p < .01$, ***$p < .001$.

amplitude of N1000cc and the number of targets when the numerosity exceeds the OI range.

Similar results were found in the analysis of tCDA. We first conducted a one-way repeated measures ANOVA on the amplitude of tCDA of conditions 1 to 6, showing a significant main effect of numerosity ($F_{(2.962,\ 79.962)} = 9.223$, $p < .001$, $\eta^2_p = .255$). Post-hoc analysis showed significant differences between 1 and other number levels ($ps < .05$). Similarly, in subsequent analyses, we divided numerosity levels into two ranges: 1–3 and 4–6. Analysis within the OI range showed a significant main effect of numerosity ($F_{(2,\ 54)} = 20.697$, $p < .001$, $\eta^2_p = .434$), with further analysis suggesting significant differences between 1 ($M = -1.459$, $SE = .412$) and 2 ($M = -2.831$, $SE = .621$) (t (27) = 3.915, $p = .002$, Cohen's $d = .740$), 2 and 3 ($M = -3.536$, $SE = .569$) (t (27) = 2.653, $p = .040$, Cohen's $d = .501$), and 1 and 3 (t (27) = 5.762, $p < .001$, Cohen's $d = .1.089$). As the numerosity increased, there was a corresponding gradual increase in the amplitude of the tCDA. Consistent with our hypothesis, the analysis conducted outside the OI range revealed no significant main effect of numerosity (p .05), indicating that the relationship between numerosity and tCDA amplitude is specific to the OI range (Fig. 6).

In Experiment 2, we continued to use the same bilateral central area electrodes, specifically FC3/4, FC5/6, C3/4, C5/6, CP3/4, and CP5/6, to measure the amplitudes on the ipsilateral and contralateral sides of the target, employing the same time windows: 900–1200 msec and 1500–1800 msec. A sustained contralateral negativity was observed during the late post-stimulus interval. To quantify the lateralized activity, we calculated difference waves by subtracting the average amplitude at contralateral electrodes from that at ipsilateral electrodes and tested the resulting amplitudes against zero using one-sample t-tests. Significant contralateral negativities were observed in both the N1000cc time window ($t(26) = -2.891$, $p = .008$, Cohen's $d = .556$) and the later maintenance-related time window ($t(26) = -3.687$, $p = .001$, Cohen's $d = .710$).

Despite the presence of reliable lateralized activity, repeated-measures ANOVAs revealed no significant main effect of numerosity in either time window (Fig. 7F). Thus, unlike Experiment 1, the amplitudes of these lateralized components did not vary systematically with the number of tactile objects. This suggests that when participants engaged in the target discrimination task, which did not depend on OI processes, the number-dependent modulation observed during tactile enumeration was absent.

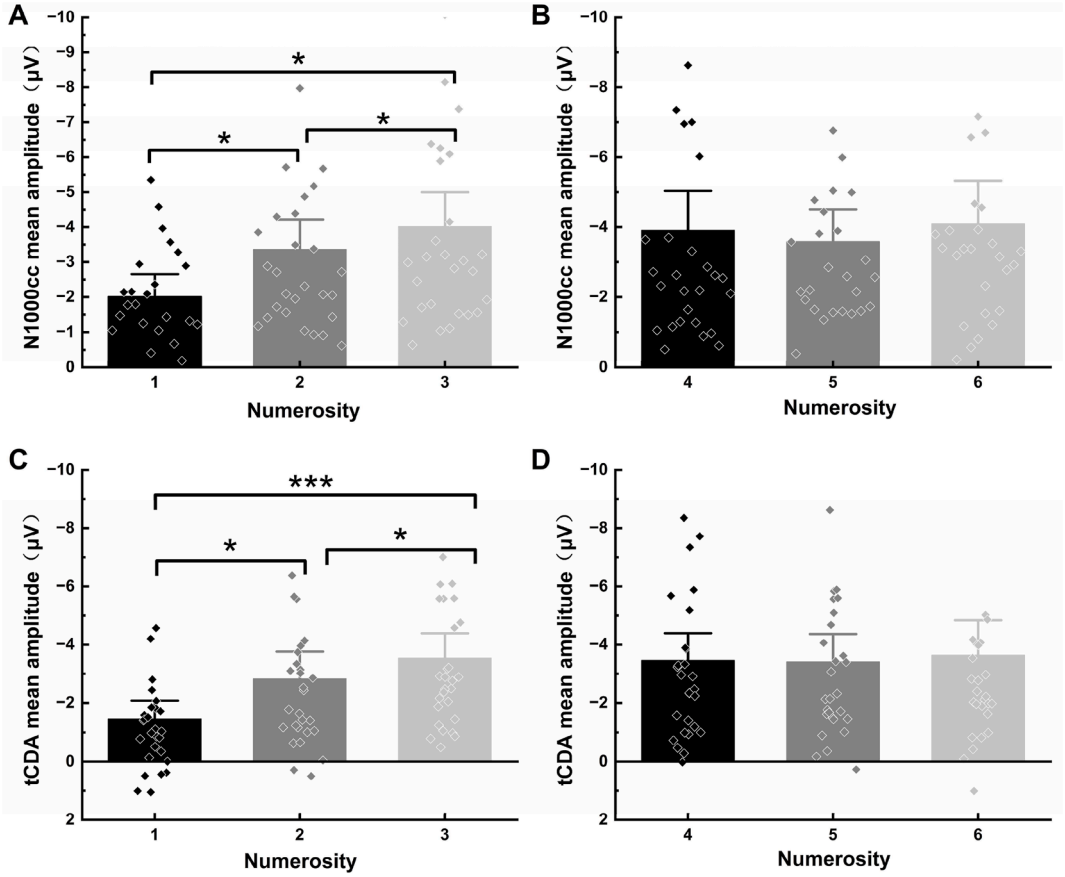

Fig. 6 – Amplitudes of N1000cc and tCDA across different numerosity levels in Experiment 1. Group and individual means of N1000cc and tCDA amplitudes, including N1000cc amplitudes within (A) and outside (B) the OI range across different numerosity levels, tCDA amplitudes within (C) and outside (D) the OI range across different numerosity levels. Bar plots and diamonds represented group means and individual data respectively, and error bars indicated standard errors of mean. *$p < .05$, **$p < .01$, ***$p < .001$.

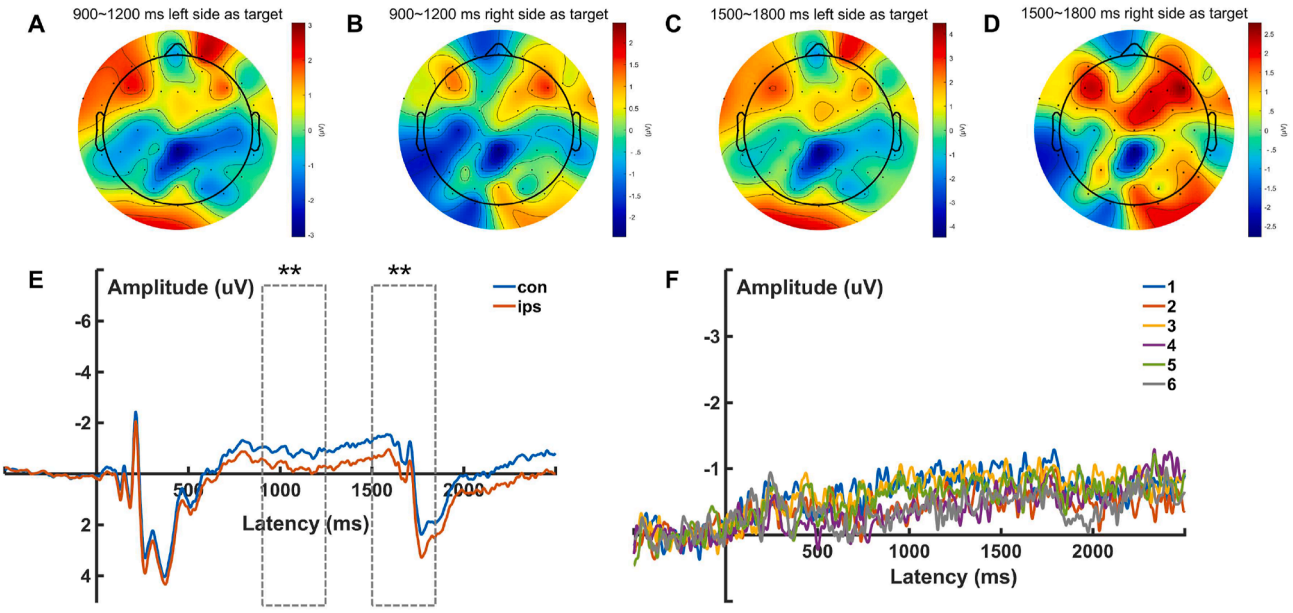

Fig. 7 – ERP results for Experiment 2. (A–D) Scalp distributions of ERP amplitude for different time windows and target conditions. (E) Differences in ERP amplitudes between contralateral and ipsilateral target sides at the central electrodes. The blue and red curves represented the average amplitudes of 1~6 for contralateral and ipsilateral target sides. (F) Difference wave amplitudes for the 1–6 levels at the central electrodes. **$p < .01$.

Importantly, although the late contralateral activity occurred within the same temporal interval as the tCDA identified in Experiment 1, its scalp distribution differed from the more focal somatosensory pattern reported in previous tactile working-memory studies (Katus & Eimer, 2015a; Katus et al., 2015b), Katus et al., 2015bnd we thus refer to it as a late lateralized maintenance-related process.

3.5. *Alpha band power decoding and time generalization*

We also conducted decoding of the number of target stimuli using alpha band power for conditions within (1–3) and outside (4–6) the OI range separately in Experiments 1 and 2. The results, as illustrated in Fig. 8, demonstrate that beginning at 940 msec after the target presentation, the decoding accuracy within the OI range of Experiment 1 significantly exceeded the chance level (cluster $p < 10^4$). This indicates that from 940 msec onward, different numerosity levels could be discerned based on the participants' alpha band power. Conversely, such high decoding accuracy was not observed outside the OI range of either Experiment 1 or Experiment 2. More importantly, decoding accuracy did not significantly differ from chance level within the OI range of Experiment 2. This collective evidence strongly suggests that the high decoding accuracy observed in the OI range of Experiment 1 was primarily attributable to the tactile OI process and not influenced by the impact of stimulus-driven sensory encoding related to non-numerical physical stimulus factors.

Subsequently, we computed a temporal generalization matrix for the decoding based on alpha band power. The cross-time-point decoding results reveal that from 940 msec to 2000 msec post-target presentation, participants developed a relatively stable neural template. This stability is evidenced by the emergence of a significant square-like region in the temporal generalization statistical outcomes (see Fig. 9).

3.6. *Alpha oscillation*

In Experiment 1, we acquired time-frequency information from all brain electrodes using the STFT method. Based on the ERP decoding results, which indicated that OI-related processing was minimally influenced by non-numerical physical stimulus properties after 860 msec, and in conjunction with the stimulus duration of 1500 msec, we selected two time windows for the analysis of alpha-band oscillatory power. One window corresponded to the stimulus presentation period (1000–1500 msec), and the other corresponded to the post-stimulus period following stimulus offset (1500–2000 msec). To facilitate direct comparisons between these two processing stages, the two time windows were defined to have equal durations. The selected time windows are illustrated in Fig. 10A and B. The STFT results from one participant were found to exceed three standard deviations from the mean. Consequently, we proceeded with the time-frequency analysis using 27 valid datasets. In addition, we also separated the data for the left and right hands and performed lateralization analyses (see Supplementary Figs. S3–S5).

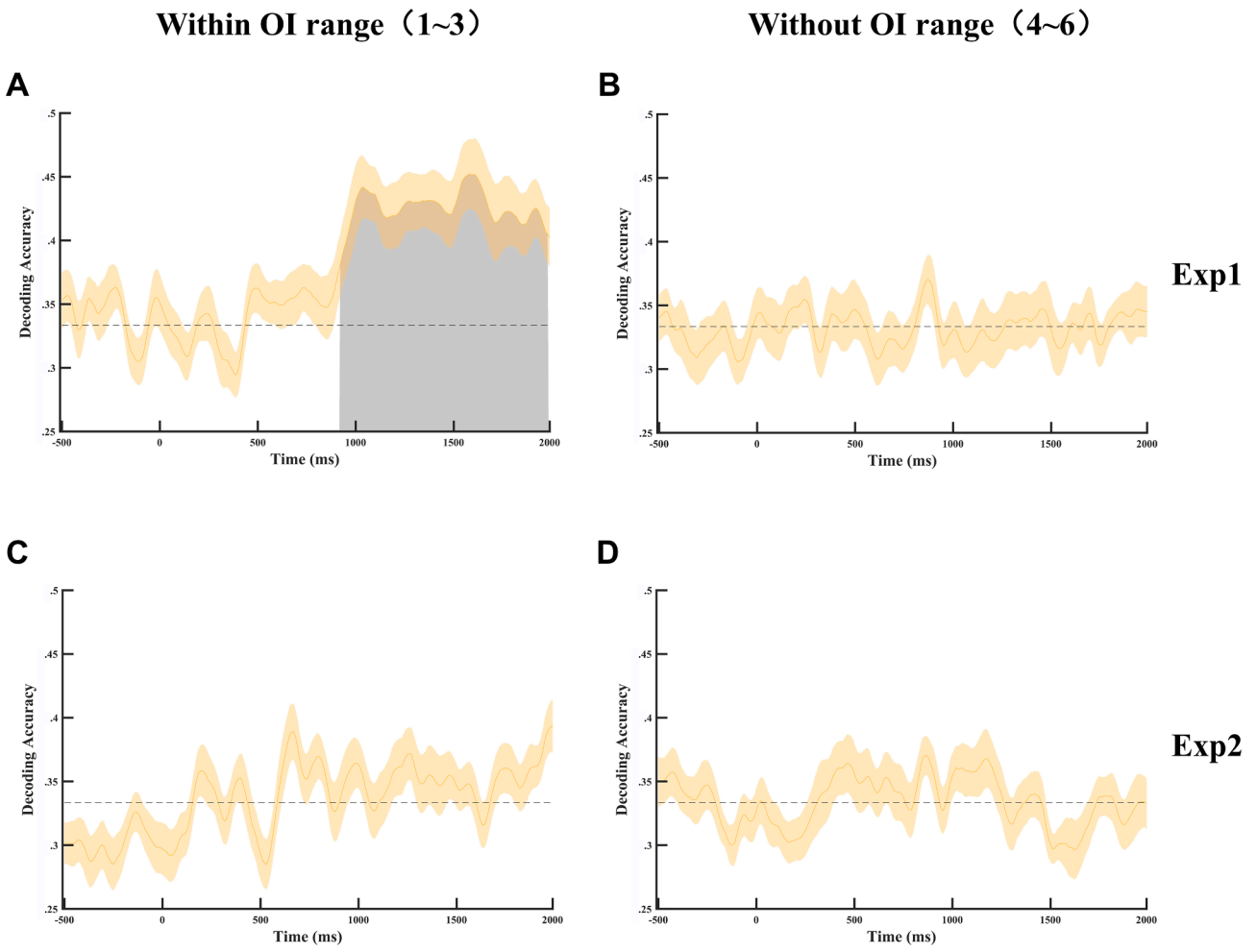

Fig. 8 – Decoding accuracy based on alpha band power for Experiment 1 and Experiment 2. Left panels showed the decoding accuracy within the OI range using alpha band power under 1–3 conditions from Experiment 1 (A) and Experiment 2 (C). Right panels showed decoding accuracy outside the OI range using alpha band power under 4–6 conditions from Experiment 1 (B) and Experiment 2 (D). Gray shading indicated time points with significant cluster permutation results. The black dashed line represented the chance level of 1/3.

We initially performed a one-way repeated measures ANOVA on the alpha band power across conditions 1 to 6 within the two specified time windows. The analysis revealed that the main effect of numerosity was non-significant across all three electrode clusters (F cluster, C cluster, and P cluster). Subsequently, we categorized the numerosity levels into two ranges: 1–3 and 4–6. Further analysis showed that the main effects of numerosity were non-significant both within and outside the OI range. Finally, we conducted paired *t*-tests to compare mean values within and outside the OI range. As depicted in Fig. 11, during the 1000–1500 msec interval, the F cluster exhibited significantly higher alpha band power within the OI range ($M = .753$, $SE = .242$) compared to outside the OI range ($M = .523$, $SE = .234$), with $t(26) = 3.128$, $p = .004$, Cohen's $d = .602$. A similar pattern was observed in the C cluster, where the alpha band power within the OI range ($M = .613$, $SE = .247$) was significantly higher than outside ($M = .421$, $SE = .247$), with $t(26) = 2.793$, $p = .010$, Cohen's $d = .537$. During the 1500–1800 msec interval, both the F cluster ($t(26) = 2.618$, $p = .015$, Cohen's $d = .504$) and the C cluster ($t(26) = 3.459$, $p = .002$, Cohen's $d = .666$) demonstrated stronger alpha band power within the OI range (F cluster: $M = .808$, $SE = .243$; C cluster: $M = .681$, $SE = .253$) relative to outside the OI range (F cluster: $M = .530$, $SE = .269$; C cluster: $M = .404$, $SE = .251$). However, in the P cluster, there was no significant difference in alpha band power between the OI range and outside the OI range. Because the OI range corresponds to the numerosity range typically associated with subitizing, whereas larger numerosities are generally processed through approximate numerical estimation supported by the ANS (Burr et al., 2010; Dehaene & Changeux, 1993; Gallistel & Gelman, 1992), we further examined whether alpha power differed between these two processing ranges. Alpha power was higher within the OI range than outside the OI range, suggesting that tactile enumeration within the individuation capacity range is associated with enhanced alpha-band activity. This pattern is

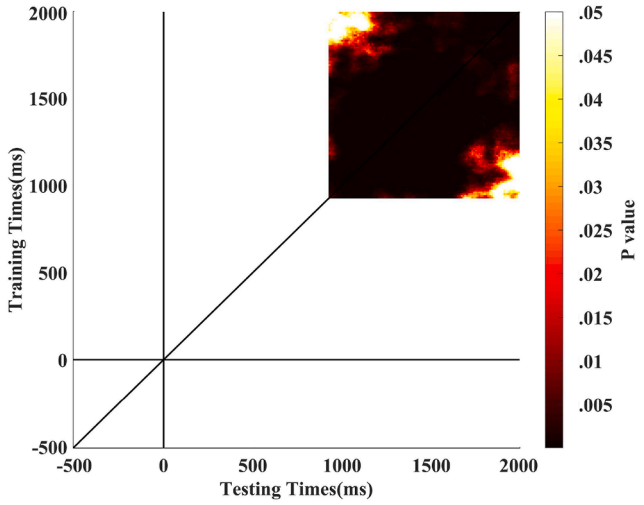

Fig. 9 – Time generalization results of alpha band power for Experiment 1. Highlighted time points represented clusters that were significant after FDR correction. The significant square-shaped regions indicated a stable neural coding pattern, with the side length of the square representing the duration of that pattern.

consistent with previous findings from MOT studies showing that alpha oscillations are modulated by object-based attentional processing (Wutz et al., 2020).

In Experiment 2, we similarly acquired time-frequency information from all brain electrodes using the STFT method, covering a time span from −500 to 2500 msec (with a step of 1 msec) and a frequency range of 1–30 Hz (with a step of 1 Hz). The adjusted time-frequency maps revealed elevated power in the alpha band (8–12 Hz, see Fig. 10C and D). We then analyzed the alpha band power in the F, C, and P regions during the time windows of 1000–1500 msec and 1500–2000 msec. The findings aligned with our hypothesis: when participants engaged in the target discrimination task, despite using the same physical stimuli as in Experiment 1, there were no significant differences in alpha band power between the small and large number ranges.

4. Discussion

In recent years, there has been a surge in research interest regarding the neural mechanisms of OI (Christophel et al., 2018; Howe et al., 2009; Hu et al., 2021; Naughtin et al., 2018; Pennock et al., 2021; Shea, 2020; Ward et al., 2021; Wurm et al., 2019). However, the majority of this evidence is derived from visual modality, with tactile OI research remaining comparatively limited. Investigating the neural correlates of tactile OI processes can enhance our comprehension of the overarching principles and mechanisms by which different sensory modalities process object information.

In our study, we sought to identify EEG indicators associated with the tactile OI process. To this end, we employed two complementary tasks with identical tactile stimulation but different cognitive demands: a tactile enumeration tasks in Experiment 1 and target discrimination tasks in Experiment 2. The enumeration task explicitly required object individuation, whereas the discrimination task did not involve OI and instead served as a control for stimulus-driven processing. By contrasting these two tasks, we were able to dissociate neural activity related to non-numerical physical stimulus properties from activity specifically associated with tactile OI. Using EEG decoding techniques, we identified two lateralized negative components linked to the tactile OI process: N1000cc and tCDA. The amplitudes of these components were found to be highly sensitive to changes in the number of objects during the OI process.

Furthermore, our results revealed that within OI range, there was a pronounced increase in alpha oscillation excitation compared to outside OI range. This discovery underscores

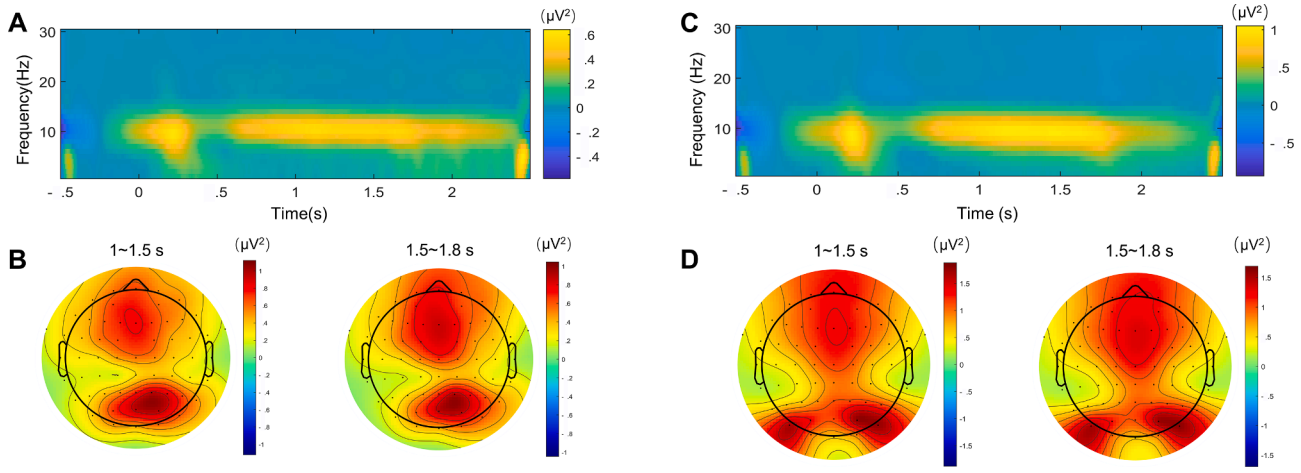

Fig. 10 – Neural oscillations during Experiment 1 and Experiment 2. Left panels showed time-frequency information of the whole brain electrodes after correction (A) and scalp distributions of alpha band power for the time windows of 1–1.5 sec (left) and 1.5–1.8 sec (right) in Experiment 1. Right panels showed the above results in Experiment 2.

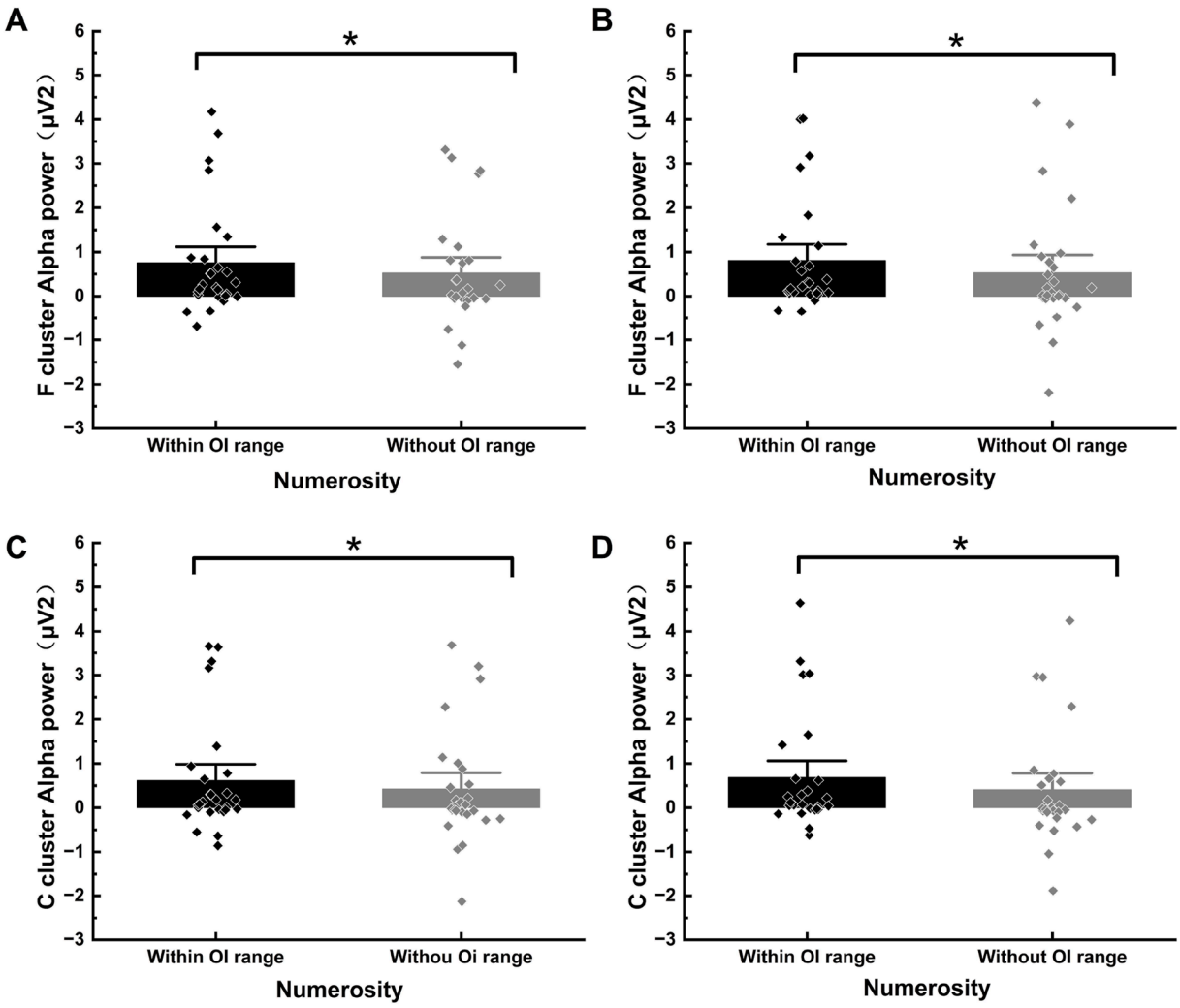

Fig. 11 – The power of the alpha band within and outside the OI range in Experiment 1. This figure showed the group and individual means of F cluster and C cluster alpha power, including F cluster alpha power within and outside OI range during 1000–1500 msec (A) and 1500–1800 msec (B), C cluster alpha power within and outside OI range during 1000–1500 msec (C) and 1500–1800 msec (D). Bar plots and diamonds represented group means and individual datarespectively, and error bars indicated standard errors. *$p < .05$.

the distinct neural signatures associated with tactile OI processes and highlights the importance of this process in tactile object perception. Our findings contribute significantly to the understanding of how tactile information is processed in the brain and offer new insights into the neural underpinnings of tactile OI.

4.1. *Object individuation is independent of non-numerical physical features*

Variations in the number of stimuli are often accompanied by changes in other non-numerical physical attributes, such as total area and density. Consequently, to demonstrate that OI is not contingent upon these continuous variables, researchers have employed various balancing techniques to reduce the impact of non-numerical physical stimuli on the OI process (Cai et al., 2021; Gebuis & Reynvoet, 2011; Piazza et al., 2011).

In our study, we used ERP signal decoding to disentangle the processing of non-numerical physical quantities from the OI process, thereby pinpointing the time periods predominantly characterized by OI activity. Our findings substantiate the notion that OI constitutes a processing mechanism that is distinct from other non-numerical continuous variables. Specifically, we identified time periods in Experiment 1 (OI task) where successful classification was achieved but could not be replicated in Experiment 2 (a target discrimination task utilizing the same stimuli as Experiment 1). We posit that the decoding success during these periods predominantly reflects tactile OI processing.

Successful decoding in both Experiment 1 and Experiment 2 was observed in a sustained window spanning 320 msec–860 msec post-stimulus. We propose that this consistent classification during the interval is influenced by

the unconscious processing of non-numerical physical information. Consequently, the time window during which successful decoding occurred in the small number range of Experiment 1 can be segmented into two distinct phases: an early phase influenced by the processing of non-numerical physical information and a later phase marked by OI processing. The time generalization results corroborate our interpretation, displaying two relatively stable signal patterns that correspond to these phases. Specifically, we identified two significant square-shaped regions in the generalization results of Experiment 1, each representing the signal activation patterns associated with the respective stages. However, it is important to note that the intersection point of the two stages (860 msec) marks the starting point where the OI process is not influenced by non-numerical physical information, but it is not the starting point of OI processing. The present results can only indicate that there is an influence of non-numerical physical information processing within the 320–860 msec, but we cannot conclude that there is no OI processing occurring during this time period. In other words, our findings do not determine the exact onset time of OI processing, and we will further discuss this issue in future research.

In sum, our study delineates two distinct phases within the decoding time window of Experiment 1: an early phase impacted by non-numerical physical information processing and a later phase dominated by OI processing, with time generalization results validating this bifurcation through the identification of two stable signal patterns. The result supports the view that OI is a process that is relatively independent of non-numerical physical information processing.

One related question concerns why comparable stimulus-driven decoding was not observed outside the OI range, despite continued covariation between numerosity and low-level tactile features (e.g., contact area, spatial extent) in that range. We suggest that early decoding reflects sensory encoding constrained by perceptual separability rather than a direct linear readout of physical stimulus differences: as spatial overlap increases and individual stimulation patterns become less distinguishable at higher numerosities, the neural discriminability of these physical attributes is correspondingly reduced. This account is consistent with the broader capacity-limited profile reported throughout our results, rather than introducing a separate mechanism specific to decoding.

It is important to note that the present behavioral results do not provide unequivocal evidence for classical tactile subitizing. Unlike visual enumeration, error rates increased monotonically with numerosity and did not exhibit a clear behavioral breakpoint. However, previous tactile studies have similarly reported that small-number advantages are often weaker and more dependent on stimulus configuration than in vision (Plaisier et al., 2009, 2010; Plaisier & Smeets, 2011). Therefore, the absence of a sharp behavioral discontinuity does not necessarily imply the absence of capacity-limited individuation-related processes.

4.2. *Critical role of attention in tactile object individuation*

To eliminate the influence of non-numerical physical quantities, we deliberately excluded the earlier lateralized component N2cc from further analysis. Instead, we concentrated on two lateralized components within a time window where the impact of non-numerical physical quantities processing was minimized: N1000cc, which peaks between 900 and 1200 msec, and tCDA, which peaks between 1500 and 1800 msec. Further analysis showed that the amplitudes of N1000cc and tCDA increased with the number of OI levels and reached their peak within the OI capacity range. This positive correlation was absent in the tactile target discrimination task, which does not engage the OI process. These findings align with the performance of neural indices related to the visual OI process, such as N2pc and CDA, as reported in previous studies (Mazza & Caramazza, 2011, 2015; Naughtin et al., 2016; Pagano et al., 2014). This correspondence suggests that N1000cc and tCDA serve as neural indices associated with the tactile OI process.

A more direct comparison with the visual literature, however, reveals both functional parallels and important differences. In visual subitizing and OI tasks, N2pc typically peaks around 200–300 msec post-stimulus over posterior contralateral scalp regions, and CDA onsets around 300–400 msec with a sustained negativity over occipito-parietal electrodes (Mazza & Caramazza, 2011, 2015; Pagano et al., 2014; Vogel & Machizawa, 2004). Both components increase in amplitude with the number of individuated objects up to the visual OI capacity limit of approximately four items. The present N1000cc and tCDA show a qualitatively similar load-dependent profile within the tactile OI range, but differ from their putative visual counterparts in three respects. First, they emerge substantially later: N1000cc peaks between 900 and 1200 msec, and tCDA between 1500 and 1800 msec post-stimulus, far exceeding the latencies of N2pc and CDA. Second, they are maximal over centroparietal rather than occipito-parietal regions, consistent with the somatosensory topography of tactile processing (Katus & Eimer, 2015a; Katus et al., 2015b). Third, the capacity limit indicated by the amplitude plateau differs: whereas visual CDA plateaus at approximately four items, the present components plateau at three items, consistent with a reduced individuation capacity in touch relative to vision (Plaisier et al., 2009; Riggs et al., 2006). These differences caution against treating N1000cc and tCDA as straightforward tactile homologues of N2pc and CDA. Because the present study did not include a matched visual condition analyzed with identical procedures, we cannot determine whether the functional parallels reflect shared supramodal individuation mechanisms or distinct modality-specific processes that produce superficially similar load-dependent profiles. Future studies employing matched cross-modal paradigms will be necessary to resolve this question.

The spatial distribution of the Experiment 1 late contralateral negativity was consistent with previous tactile CDA studies (Katus & Eimer, 2015a; Katus et al., 2015b),as the effect

was quantified from a centroparietal electrode cluster and showed maximal contralateral activity over central scalp regions. In contrast, the corresponding activity in Experiment 2 was less spatially focal, possibly reflecting the reduced object-based attentional and maintenance demands of the temporal detection task. Similar reductions in the spatial specificity of lateralized activity have been reported under lower memory-load conditions (Katus et al., 2015b). Thus, Experiment 2 provides converging but weaker evidence for tactile CDA-like activity, whereas Experiment 1 provides the primary evidence linking late lateralized activity to tactile object individuation.

These load-dependent effects are unlikely to reflect general task difficulty or sustained attention alone. A pure difficulty account predicts monotonic modulation scaling with demand across both experiments and all numerosity levels; instead, we observed a nonlinear profile in which amplitude increases within the OI range and then reaches a plateau beyond it, specific to Experiment 1. Likewise, sustained attention typically produces gradual, condition-general modulation, whereas the present effects showed a sharp temporal transition around 860 msec confined to the OI-relevant range, arguing against a purely attentional account. Motor preparation is similarly unlikely to account for these effects, as responses were collected only after a fixed post-stimulus delay (~3.5 sec), well beyond the analyzed ERP windows.

Although the present paradigm did not employ the delayed-match-to-sample design used by Katus et al. (2015b), an N2cc-like early lateralized negativity (250–550 msec) was observed and showed a load-related increase within the OI range (1–3 items), consistent with earlier reports of early attentional selection in tactile working memory. However, this effect did not extend across all numerosity levels, suggesting that N2cc does not reliably track numerosity beyond the OI capacity range. In addition, decoding results indicated substantial stimulus-driven processing during the early interval (320–860 msec), raising the possibility that the observed modulation partly reflects sensory encoding differences rather than individuation-specific selection. These findings suggest that early lateralized activity may be confounded by perceptual processing demands, whereas later components provide a more stable index of tactile object individuation in the present paradigm. In previous studies, lateralized components have typically been associated with the allocation of spatial attention, as seen with N2pc and N2cc (Forster et al., 2016; Gherri et al., 2021; Mena et al., 2020). The N1000cc and tCDA identified in our study were also lateralized components. Compared to the target side, the negative amplitudes of N1000cc and tCDA on the non-target side were larger. Consequently, N1000cc and tCDA also appear to reflect the distinction between attended and unattended sides, signifying the allocation of tactile spatial attention.

Consequently, the amplitudes of the lateralized components, N1000cc and tCDA, effectively differentiate between various OI levels. This provides robust evidence for the attention-dependent nature of the tactile OI process, consistent with evidence from the visual modality showing that subitizing requires attention (Olivers & Watson, 2008).

4.3. *Unveiling the OI process: target location enhancement and non-target suppression*

The time-frequency analysis revealed that during the time windows of 1–1.5 sec and 1.5–1.8 sec post-stimulus presentation, the alpha band power within the OI range was significantly elevated compared to that outside the OI range in Experiment 1. This finding aligns with prior research on the visual OI process (Noguchi & Kakigi, 2020; Wutz et al., 2020). Furthermore, our findings demonstrated that different OI levels could be accurately distinguished based on the alpha band power of participants. As anticipated, this variation in alpha oscillation power was not observed in Experiment 2. It is important to highlight that while previous studies on the OI process have largely reported alpha oscillations in the parieto-occipital lobe (Babu Henry Samuel et al., 2018; Noguchi & Kakigi, 2020; Wang et al., 2018), our research predominantly detected these oscillations in the frontal and central regions. This divergence may stem from the distinct brain areas engaged in processing visual versus tactile stimuli. Prior investigations into neural oscillations related to OI have been heavily focused on the visual modality, which explains the prevalence of occipital lobe findings. In contrast, studies examining neural oscillations linked to tactile working memory and analogous tactile processes typically report alpha oscillation activation in the frontal (Spitzer & Blankenburg, 2011; Van Ede et al., 2017), and central (Esmaeili & Diamond, 2019) regions.

Some researchers suggested that alpha oscillations are instrumental in focusing attention on critical locations by inhibiting distracting stimuli, thereby enhancing the separation of target objects from the background (Babu Henry Samuel et al., 2018; Jensen, 2002; Noguchi & Kakigi, 2020). During the OI process, target objects are identified based on their spatial information. Thus, alpha oscillations are vital for suppressing irrelevant stimuli to highlight or guide attention to the locations that correspond to the number of target objects (Wutz et al., 2020). In contrast, when the object number outside the OI range, individuals will adopt an approximate representation strategy, a holistic approximation is used where all target objects are perceived as a single entity, and differentiation based on location is unnecessary (Trick & Pylyshyn, 1994; Xu & Chun, 2009). In this case, alpha oscillations only need to suppress distractions and direct attention to the entire set of target objects. Consequently, in our study, we observed stronger alpha oscillations within OI range compared to outside OI range, indicating a greater need for attentional allocation across multiple locations within the OI range. Additionally, the power of alpha oscillations varied at different OI levels, reflecting the varying number of positions that required attentional emphasis.

4.4. *Limitations*

Several limitations of the present study should be noted. First, the temporal windows used for ERP analyses were partially informed by decoding results from Experiment 1 and therefore cannot be considered fully independent a priori definitions; the temporal specificity of the ERP effects should

accordingly be interpreted as hypothesis-guided rather than strictly confirmatory. Second, because numerosity covaried with stimulated area, spatial extent, and local density, the present design cannot fully dissociate numerosity from correlated physical stimulus properties, despite the cross-experiment comparison allowing isolation of OI-specific neural activity. Future studies should orthogonally manipulate numerosity and continuous tactile variables to determine their respective contributions.

At the level of interpretation, two further issues remain open. The load-dependent profile of the late contralateral activity argues against accounts based solely on task difficulty, sustained attention, or motor preparation, but these remain indirect arguments from converging patterns rather than direct causal evidence; establishing causal specificity will require interventional approaches such as TMS. That is to say, while the N1000cc and tCDA track the number of individuated objects, future research using neuromodulation (e.g., TMS) or clinical models would be necessary to establish a formal causal link between these components and tactile OI performance. Additionally, whether the decoding effects reflect lateralized or non-lateralized numerosity processing cannot be resolved here, as block-level counterbalancing of target hand confounds any cross-hand generalization analysis with between-block variability. Future within-block counterbalancing designs would allow this to be addressed directly.

5. Conclusion

In conclusion, our study has identified two neural markers associated with the tactile object individuation process: N1000cc and tCDA. A key highlight is that the amplitudes of these components not only increased with the number of OI items but also reached a peak within the OI capacity range, demonstrating a clear task-specific positive correlation. Furthermore, paralleling the visual OI process, we observed heightened alpha oscillation power within tactile OI range as opposed to outside OI range. These novel insights significantly advance our comprehension of the tactile modality's processing mechanisms for object individuation.

Scientific transparency statement

DATA: All raw and processed data supporting this research are publicly available: https://disk.pku.edu.cn/link/AAD499440195BE4094AC30B78C6C4035F1.or https://ngdc.cncb.ac.cn/omix/release/OMIX019880.

CODE: All analysis code supporting this research is publicly available: https://disk.pku.edu.cn/link/AAD499440195BE4094AC30B78C6C4035F1.or https://ngdc.cncb.ac.cn/omix/release/OMIX019880.

MATERIALS: All study materials supporting this research are publicly available: https://disk.pku.edu.cn/link/AAD499440195BE4094AC30B78C6C4035F1.or https://ngdc.cncb.ac.cn/omix/release/OMIX019880.

DESIGN: This article reports, for all studies, how the author(s) determined all sample sizes, all data exclusions, all data inclusion and exclusion criteria, and whether inclusion and exclusion criteria were established prior to data analysis.

PRE-REGISTRATION: No part of the study procedures was pre-registered in a time-stamped, institutional registry prior to the research being conducted. No part of the analysis plans was pre-registered in a time-stamped, institutional registry prior to the research being conducted.

For full details, see the *Scientific Transparency Report* in the supplementary data to the online version of this article.

CRediT authorship contribution statement

Chunmiao Lou: Writing – review & editing, Writing – original draft, Visualization, Methodology, Investigation, Formal analysis, Data curation. **Yang Lei:** Writing – review & editing, Writing – original draft, Methodology, Formal analysis. **Uta Noppeney:** Writing – review & editing, Methodology. **Lihan Chen:** Writing – review & editing, Writing – original draft, Validation, Supervision, Resources, Project administration, Methodology, Funding acquisition, Conceptualization.

Author note

We declare no conflict of interest in this research. Data and analysis Matlab scripts are available at: https://disk.pku.edu.cn/link/AAD499440195BE4094AC30B78C6C4035F1. or at:https://ngdc.cncb.ac.cn/omix/release/OMIX019880.

Financial support

The STI2030-Major Project (2021ZD0202600) and Natural Science Foundation of China (T2192932) to L.C.

Supplementary data

Supplementary data to this article can be found online at https://doi.org/10.1016/j.cortex.2026.08.014.

REFERENCES

Anobile, G., Arrighi, R., & Burr, D. C. (2019). Simultaneous and sequential subitizing are separate systems, and neither predicts math abilities. *Journal of Experimental Child Psychology, 178*, 86–103. https://doi.org/10.1016/j.jecp.2018.09.017

Anobile, G., Arrighi, R., Castaldi, E., & Burr, D. C. (2021). A sensorimotor numerosity system. *Trends in Cognitive Sciences, 25*(1), 24–36. https://doi.org/10.1016/j.tics.2020.10.009

Anobile, G., Turi, M., Cicchini, G. M., & Burr, D. C. (2012). The effects of cross-sensory attentional demand on subitizing and on mapping number onto space. *Vision Research, 74*, 102–109. https://doi.org/10.1016/j.visres.2012.06.005

Ansari, D. (2008). Effects of development and enculturation on number representation in the brain. *Nature Reviews Neuroscience, 9*(4), 278–291. https://doi.org/10.1038/nrn2334

Babu Henry Samuel, I., Wang, C., Hu, Z., & Ding, M. (2018). The frequency of alpha oscillations: Task-dependent modulation

and its functional significance. *Neuroimage, 183*, 897–906. https://doi.org/10.1016/j.neuroimage.2018.08.063
Bae, G.-Y., & Luck, S. J. (2018). Dissociable decoding of spatial attention and working memory from EEG oscillations and sustained potentials. *The Journal of Neuroscience, 38*(2), 409–422. https://doi.org/10.1523/JNEUROSCI.2860-17.2017
Bae, G.-Y., & Luck, S. J. (2019). Reactivation of previous experiences in a working memory task. *Psychological Science, 30*(4), 587–595. https://doi.org/10.1177/0956797619830398
Brainard, D. H. (1997). The psychophysics toolbox. *Spatial Vision, 10*(4), 433–436. https://doi.org/10.1163/156856897X00357
Burr, D. C., Turi, M., & Anobile, G. (2010). Subitizing but not estimation of numerosity requires attentional resources. *Journal of Vision, 10*(6), 20. https://doi.org/10.1167/10.6.20
Cai, Y., Hofstetter, S., van Dijk, J., Zuiderbaan, W., van der Zwaag, W., Harvey, B. M., & Dumoulin, S. O. (2021). Topographic numerosity maps cover subitizing and estimation ranges. *Nature Communications, 12*(1), 3374. https://doi.org/10.1038/s41467-021-23785-7
Chesney, D. L., & Haladjian, H. H. (2011). Evidence for a shared mechanism used in multiple-object tracking and subitizing. *Attention, Perception, & Psychophysics, 73*(8), 2457–2480. https://doi.org/10.3758/s13414-011-0204-9
Christophel, T. B., Iamshchinina, P., Yan, C., Allefeld, C., & Haynes, J.-D. (2018). Cortical specialization for attended versus unattended working memory. *Nature Neuroscience, 21*(4), 494–496. https://doi.org/10.1038/s41593-018-0094-4
Cicchini, G. M., Anobile, G., & Burr, D. C. (2016). Spontaneous perception of numerosity in humans. *Nature Communications, 7*(1), Article 12536. https://doi.org/10.1038/ncomms12536
Cohen, Z. Z., Aisenberg, D., & Henik, A. (2018). The effects of training on tactile enumeration. *Psychological Research, 82*(3), 468–487. https://doi.org/10.1007/s00426-016-0835-5
Cohen, Z. Z., Arend, I., Yuen, K., Naparstek, S., Gliksman, Y., Veksler, R., & Henik, A. (2018). Tactile enumeration: A case study of acalculia. *Brain and Cognition, 127*, 60–71. https://doi.org/10.1016/j.bandc.2018.10.001
Cohen, Z. Z., & Henik, A. (2016). Effects of numerosity range on tactile and visual enumeration. *Perception, 45*(1–2), 83–98. https://doi.org/10.1177/0301006615614662
Dehaene, S., & Changeux, J.-P. (1993). Development of elementary numerical abilities: A neuronal model. *Journal of Cognitive Neuroscience, 5*(4), 390–407. https://doi.org/10.1162/jocn.1993.5.4.390
Delorme, A., & Makeig, S. (2004). EEGLAB: An open source toolbox for analysis of single-trial eeg dynamics including independent component analysis. *Journal of Neuroscience Methods, 134*, 9–21.
Dietterich, T. G., & Bakiri, G. (1994). Solving multiclass learning problems via error-correcting output codes. *Journal of Artificial Intelligence Research, 2*, 263–286.
Drew, T., Horowitz, T. S., Wolfe, J. M., & Vogel, E. K. (2012). Neural measures of dynamic changes in attentive tracking load. *Journal of Cognitive Neuroscience, 24*(2), 440–450. https://doi.org/10.1162/jocn_a_00107
Drew, T., & Vogel, E. K. (2008). Neural measures of individual differences in selecting and tracking multiple moving objects. *Journal of Neuroscience, 28*(16), 4183–4191. https://doi.org/10.1523/JNEUROSCI.0556-08.2008
Eger, E., Michel, V., Thirion, B., Amadon, A., Dehaene, S., & Kleinschmidt, A. (2009). Deciphering cortical number coding from human brain activity patterns. *Current biology, 19*(19), 1608–1615. https://doi.org/10.1016/j.cub.2009.08.047
Esmaeili, V., & Diamond, M. E. (2019). Neuronal correlates of tactile working memory in prefrontal and vibrissal somatosensory cortex. *Cell Reports, 27*(11), 3167–3181.e5. https://doi.org/10.1016/j.celrep.2019.05.034
Faul, F., Erdfelder, E., Lang, A.-G., & Buchner, A. (2007). G*Power 3: A flexible statistical power analysis program for the social, behavioral, and biomedical sciences. *Behavior Research Methods, 39*(2), 175–191. https://doi.org/10.3758/BF03193146
Feldmann-Wüstefeld, T. (2021). Neural measures of working memory in a bilateral change detection task. *Psychophysiology, 58*(1). https://doi.org/10.1111/psyp.13683
Forster, B., Tziraki, M., & Jones, A. (2016). The attentive homunculus: ERP evidence for somatotopic allocation of attention in tactile search. *Neuropsychologia, 84*, 158–166. https://doi.org/10.1016/j.neuropsychologia.2016.02.009
Gallace, A., Tan, H. Z., & Spence, C. (2006). Numerosity judgments for tactile stimuli distributed over the body surface. *Perception, 35*(2), 247–266. https://doi.org/10.1068/p5380
Gallace, A., Tan, H. Z., & Spence, C. (2008). Can tactile stimuli be subitised? An unresolved controversy within the literature on numerosity judgments. *Perception, 37*(5), 782–800. https://doi.org/10.1068/p5767
Gallistel, C. R., & Gelman, R. (1992). Preverbal and verbal counting and computation. *Cognition, 44*(1–2), 43–74. https://doi.org/10.1016/0010-0277(92)90050-R
Gebuis, T., & Reynvoet, B. (2011). Generating nonsymbolic number stimuli. *Behavior Research Methods, 43*(4), 981–986. https://doi.org/10.3758/s13428-011-0097-5
Gherri, E., Zhao, B., & Ambron, E. (2021). Behavioural and electrophysiological evidence for the effect of target-distractor separation in a tactile search task. *Biological Psychology, 162*, Article 108098. https://doi.org/10.1016/j.biopsycho.2021.108098
Göddertz, A., Klatt, L.-I., Mertes, C., & Schneider, D. (2018). Retroactive attentional shifts predict performance in a working memory task: Evidence by lateralized EEG patterns. *Frontiers in Human Neuroscience, 12*, 428. https://doi.org/10.3389/fnhum.2018.00428
Groppe, D. M., Urbach, T. P., & Kutas, M. (2011). Mass univariate analysis of event-related brain potentials/fields I: A critical tutorial review. *Psychophysiology, 48*(12), 1711–1725. https://doi.org/10.1111/j.1469-8986.2011.01273.x
Gui, P., Ku, Y., Li, L., Li, X., Bodner, M., Lenz, F. A., Wang, L., & Zhou, Y.-D. (2017). Neural correlates of visuo-tactile crossmodal paired-associate learning and memory in humans. *Neuroscience, 362*, 181–195. https://doi.org/10.1016/j.neuroscience.2017.08.035
Hochman, S., Cohen, Z. Z., Ben-Shachar, M. S., & Henik, A. (2020). Tactile enumeration and embodied numerosity among the deaf. *Cognitive Science, 44*(8). https://doi.org/10.1111/cogs.12880
Howe, P. D., Horowitz, T. S., Akos Morocz, I., Wolfe, J., & Livingstone, M. S. (2009). Using fMRI to distinguish components of the multiple object tracking task. *Journal of Vision, 9*(4), 10. https://doi.org/10.1167/9.4.10, 10.
Hu, L., Cai, M. M., Xiao, P., Luo, F., & Iannetti, G. D. (2014). Human brain responses to concomitant stimulation of Aδ and C nociceptors. *The Journal of Neuroscience, 34*(34), 11439–11451. https://doi.org/10.1523/JNEUROSCI.1355-14.2014
Hu, L., Wang, C., Talhelm, T., & Zhang, X. (2021). Distinguishing the neural mechanism of attentional control and working memory in feature-based attentive tracking. *Psychophysiology, 58*(2). https://doi.org/10.1111/psyp.13726
Hu, Z., Barkley, C. M., Marino, S. E., Wang, C., Rajan, A., Bo, K., Samuel, I. B. H., & Ding, M. (2019). Working memory capacity is negatively associated with memory load modulation of alpha oscillations in retention of verbal working memory. *Journal of Cognitive Neuroscience, 31*(12), 1933–1945. https://doi.org/10.1162/jocn_a_01461
Jensen, O. (2002). Oscillations in the alpha band (9-12 Hz) increase with memory load during retention in a short-term memory task. *Cerebral Cortex, 12*(8), 877–882. https://doi.org/10.1093/cercor/12.8.877

Jensen, O., Gelfand, J., Kounios, J., & Lisman, J. E. (2002). Oscillations in the alpha band (9-12 Hz) increase with memory load during retention in a short-term memory task. *Cerebral cortex, 12*(8), 877–882 (New York, N.Y. : 1991) https://doi.org/10.1093/cercor/12.8.877.

Katus, T., & Eimer, M. (2015a). Lateralized delay period activity marks the focus of spatial attention in working memory: Evidence from somatosensory event-related brain potentials. *The Journal of Neuroscience, 35*(17), 6689–6695. https://doi.org/10.1523/JNEUROSCI.5046-14.2015

Katus, T., Grubert, A., & Eimer, M. (2015b). Electrophysiological evidence for a sensory recruitment model of somatosensory working memory. *Cerebral Cortex, 25*(12), 4697–4703. https://doi.org/10.1093/cercor/bhu153

King, J.-R., & Dehaene, S. (2014). Characterizing the dynamics of mental representations: The temporal generalization method. *Trends in Cognitive Sciences, 18*(4), 203–210. https://doi.org/10.1016/j.tics.2014.01.002

Kleiner, M. B., Brainard, D. H., & Pelli, D. G. (2007). What's new in Psychtoolbox-3? *Perception, 36*(2), 301–307. https://doi.org/10.1068/v070821

Li, Y., & Noguchi, Y. (2022). Neural correlates of a load-dependent decline in visual working memory. *Cerebral Cortex Communications, 3*(2), tgac015. https://doi.org/10.1093/texcom/tgac015

Lou, C., Zeng, H., & Chen, L. (2022). Asymmetric switch cost between subitizing and estimation in tactile modality. *Current Psychology*. https://doi.org/10.1007/s12144-022-02858-w

Mazza, V., & Caramazza, A. (2011). Temporal brain dynamics of multiple object processing: The flexibility of individuation. *Plos One, 6*(2), Article e17453. https://doi.org/10.1371/journal.pone.0017453

Mazza, V., & Caramazza, A. (2015). Multiple object individuation and subitizing in enumeration: A view from electrophysiology. *Frontiers in Human Neuroscience, 9*. https://doi.org/10.3389/fnhum.2015.00162

Mena, C. I., Lang, K., & Gherri, E. (2020). Electrophysiological correlates of attentional selection in tactile search tasks: The impact of singleton distractors on target selection. *Psychophysiology, 57*(9). https://doi.org/10.1111/psyp.13592

Naughtin, C. K., Mattingley, J. B., Bender, A. D., & Dux, P. E. (2018). Decoding early and late cortical contributions to individuation of attended and unattended objects. *Cortex; a Journal Devoted To the Study of the Nervous System and Behavior, 99*, 45–54. https://doi.org/10.1016/j.cortex.2017.10.013

Naughtin, C. K., Mattingley, J. B., & Dux, P. E. (2016). Early information processing contributions to object individuation revealed by perception of illusory figures. *Journal of Neurophysiology, 116*(6), 2513–2522. https://doi.org/10.1152/jn.00082.2016

Naughtin, C. K., Tamber-Rosenau, B. J., & Dux, P. E. (2017). The neural basis of temporal individuation and its capacity limits in the human brain. *Journal of Neurophysiology, 118*(5), 2601–2613. https://doi.org/10.1152/jn.00839.2016

Nieder, A. (2012). Supramodal numerosity selectivity of neurons in primate prefrontal and posterior parietal cortices. *Proceedings of the National Academy of Sciences, 109*(29), 11860–11865. https://doi.org/10.1073/pnas.1204580109

Nieder, A. (2016). The neuronal code for number. *Nature Reviews Neuroscience, 17*(6), 366–382. https://doi.org/10.1038/nrn.2016.40

Nieder, A. (2025). Numerosity coding in the brain: From early visual processing to. abstract representations. *Cerebral Cortex, 35*(7), bhaf180. https://doi.org/10.1093/cercor/bhaf180

Nieder, A., Diester, I., & Tudusciuc, O. (2006). Temporal and spatial enumeration processes in the primate parietal cortex. *Science, 313*(5792), 1431–1435. https://doi.org/10.1126/science.1130308

Noguchi, Y., & Kakigi, R. (2020). Temporal codes of visual working memory in the human cerebral cortex. *Neuroimage, 222*, Article 117294. https://doi.org/10.1016/j.neuroimage.2020.117294

Olivers, C. N. L., & Watson, D. G. (2008). Subitizing requires attention. *Visual. Cognition, 16*(4), 439–462. https://doi.org/10.1080/13506280701825861

Pagano, S., Lombardi, L., & Mazza, V. (2014). Brain dynamics of attention and working memory engagement in subitizing. *Brain Research, 1543*, 244–252. https://doi.org/10.1016/j.brainres.2013.11.025

Pagano, S., & Mazza, V. (2012). Individuation of multiple targets during visual enumeration: New insights from electrophysiology. *Neuropsychologia, 50*(5), 754–761. https://doi.org/10.1016/j.neuropsychologia.2012.01.009

Palva, S., Kulashekhar, S., Hmlinen, M., & Palva, J. M. (2011). Localization of cortical phase and amplitude dynamics during visual working memory encoding and retention. *Journal of Neuroscience the Official Journal of the Society for Neuroscience, 31*(13), 5013–5025. https://doi.org/10.1523/JNEUROSCI.5592-10.2011

Pan, Y., Tan, Z., Gao, Z., Li, Y., & Wang, L. (2018). Neural activity is dynamically modulated by memory load during the maintenance of spatial objects. *Frontiers in Psychology, 9*, 1071. https://doi.org/10.3389/fpsyg.2018.01071

Pavlov, Y. G., & Kotchoubey, B. (2022). Oscillatory brain activity and maintenance of verbal and visual working memory: A systematic review. *Psychophysiology, 59*(5). https://doi.org/10.1111/psyp.13735

Pelli, D. G. (1997). The VideoToolbox software for visual psychophysics: Transforming numbers into movies. *Spatial Vision, 10*(4), 437–442. https://doi.org/10.1163/156856897X00366

Pennock, I. M. L., Schmidt, T. T., Zorbek, D., & Blankenburg, F. (2021). Representation of visual numerosity information during working memory in humans: An FMRI decoding study. *Human Brain Mapping, 42*(9), 2778–2789. https://doi.org/10.1002/hbm.25402

Piazza, M., Fumarola, A., Chinello, A., & Melcher, D. (2011). Subitizing reflects visuo-spatial object individuation capacity. *Cognition, 121*(1), 147–153. https://doi.org/10.1016/j.cognition.2011.05.007

Plaisier, M. A., Bergmann Tiest, W., & Kappers, A. (2010). Haptic object individuation. *IEEE Transactions on Haptics, 3*(4), 257–265. https://doi.org/10.1109/TOH.2010.6

Plaisier, M. A., Bergmann Tiest, W. M., & Kappers, A. M. L. (2009). One, two, three, many – Subitizing in active touch. *Acta Psychologica, 131*(2), 163–170. https://doi.org/10.1016/j.actpsy.2009.04.003

Plaisier, M. A., & Smeets, J. B. J. (2011). Haptic subitizing across the fingers. *Attention, Perception, & Psychophysics, 73*(5), 1579–1585. https://doi.org/10.3758/s13414-011-0124-8

Poncet, M., & Chakravarthi, R. (2020). Subitizing object parts reveals a second stage of individuation. *Psychonomic Bulletin & Review*. https://doi.org/10.3758/s13423-020-01836-2

Pylyshyn, Z. (1994). Some primitive mechanisms of spatial attention. *Cognition, 50*(1–3), 363–384. https://doi.org/10.1016/0010-0277(94)90036-1

Riggs, K. J., Ferrand, L., Lancelin, D., Fryziel, L., Dumur, G., & Simpson, A. (2006). Subitizing in tactile perception. *Psychological Science, 17*(4), 271–272. https://doi.org/10.1111/j.1467-9280.2006.01696.x

Shea, B. (2020). The role of object individuation in attention and visual processing. *The Journal of Neuroscience, 40*(39), 7387–7389. https://doi.org/10.1523/JNEUROSCI.1257-20.2020

Spitzer, B., & Blankenburg, F. (2011). Stimulus-dependent EEG activity reflects internal updating of tactile working memory in humans. *Proceedings of the National Academy of Sciences, 108*(20), 8444–8449. https://doi.org/10.1073/pnas.1104189108

Su, S. Y., Chai, G. H., Sheng, X. J., Meng, J. J., & Zhu, X. Y. (2020). Contra-lateral. desynchronized alpha oscillations linearly correlate with discrimination performance of tactile acuity. *Journal of Neural Engineering, 17*(4). ARTN046041 https://doi.org/10.1088/1741-2552/aba55f.

Tian, Y., & Chen, L. (2018). Cross-modal attention modulates tactile subitizing but not. tactile numerosity estimation. *Attention, Perception & Psychophysics, 80*(5), 1229–1239. https://doi.org/10.3758/s13414-018-1507-x

Trick, L. M., & Pylyshyn, Z. W. (1994). Why are small and large numbers enumerated differently? A limited-capacity preattentive stage in vision. *Psychological Review, 101*(1), 80–102. https://doi.org/10.1037/0033-295X.101.1.80

Tu, Y., Zhang, Z., Tan, A., Peng, W., Hung, Y. S., Moayedi, M., Iannetti, G. D., & Hu, L. (2016). Alpha and gamma oscillation amplitudes synergistically predict the perception of forthcoming nociceptive stimuli: Prestimulus oscillations modulate sensory percept. *Human Brain Mapping, 37*(2), 501–514. https://doi.org/10.1002/hbm.23048

Van Ede, F., Jensen, O., & Maris, E. (2017). Supramodal theta, gamma, and sustained fields predict modality-specific modulations of alpha and beta oscillations during visual and tactile working memory. *Journal of Cognitive Neuroscience, 29*(8), 1455–1472. https://doi.org/10.1162/jocn_a_01129

Vogel, E. K., & Machizawa, M. G. (2004). Neural activity predicts individual differences in visual working memory capacity. *Nature, 428*(6984), 748–751. https://doi.org/10.1038/nature02447

Wang, C., Hu, L., Hu, S., Xu, Y., & Zhang, X. (2018). Functional specialization for feature-based and symmetry-based groupings in multiple object tracking. *Cortex; a journal devoted to the study of the nervous system and behavior*, *108*, 265–275. https://doi.org/10.1016/j.cortex.2018.09.005

Ward, R. T., Lotfi, S., Stout, D. M., Mattson, S., Lee, H.-J., & Larson, C. L. (2021). Neutral and threatening distracter word stimuli are unnecessarily stored in working memory but do not differ in their degree of working memory storage. *Biological Psychology, 162*, Article 108091. https://doi.org/10.1016/j.biopsycho.2021.108091

Wianda, E., & Ross, B. (2019). The roles of alpha oscillation in working memory retention. *Brain and Behavior, 9*(4), Article e01263. https://doi.org/10.1002/brb3.1263

Wurm, M. F., Porter, K. B., & Caramazza, A. (2019). Individuation of parts of a single object and multiple distinct objects relies on a common neural mechanism in inferior intraparietal sulcus. *Cortex; a Journal Devoted to the Study of the Nervous System and Behavior, 121*, 1–15. https://doi.org/10.1016/j.cortex.2019.08.012

Wutz, A., Zazio, A., & Weisz, N. (2020). Oscillatory bursts in parietal cortex reflect dynamic attention between multiple objects and ensembles. *The Journal of Neuroscience, 40*(36), 6927–6937. https://doi.org/10.1523/JNEUROSCI.0231-20.2020

Xu, Y. (2009). Distinctive neural mechanisms supporting visual object individuation and identification. *Journal of Cognitive Neuroscience, 21*(3), 511–518. https://doi.org/10.1162/jocn.2008.21024

Xu, Y., & Chun, M. M. (2009). Selecting and perceiving multiple visual objects. *Trends in Cognitive Sciences, 13*(4), 167–174. https://doi.org/10.1016/j.tics.2009.01.008